

**Above-threshold ionization and laser-induced electron diffraction in diatomic molecules**Noslen Suárez,<sup>1,\*</sup> Alexis Chacón,<sup>1</sup> Marcelo F. Ciappina,<sup>2,3</sup> Benjamin Wolter,<sup>1</sup> Jens Biegert,<sup>1,4</sup> and Maciej Lewenstein<sup>1,4</sup><sup>1</sup>*ICFO-Institut de Ciències Fotòniques, The Barcelona Institute of Science and Technology, Av. Carl Friedrich Gauss 3, 08860 Castelldefels (Barcelona), Spain*<sup>2</sup>*Max-Planck-Institut für Quantenoptik, Hans-Kopfermann-Str. 1, 85748 Garching, Germany*<sup>3</sup>*Institute of Physics of the ASCR, ELI-Beamlines, Na Slovance 2, 182 21 Prague, Czech Republic*<sup>4</sup>*ICREA, Pg. Lluís Companys 23, 08010 Barcelona, Spain*

(Received 26 July 2016; published 27 October 2016)

Strong-field photoemission and electron recollision provide a viable route to extract electronic and nuclear dynamics from molecular targets with attosecond temporal resolution. However, since an *ab initio* treatment of even the simplest diatomic systems is beyond today's capabilities, approximate qualitative descriptions are warranted. In this paper, we develop such a theoretical approach to model the photoelectrons resulting from intense laser-molecule interaction. We present a general theory for symmetric diatomic molecules in the single active electron approximation that, amongst other capabilities, allows adjusting both the internuclear separation and molecular potential in a direct and simple way. More importantly, we derive an analytic approximate solution of the time-dependent Schrödinger equation (TDSE), based on a generalized strong-field approximation (SFA) version. Using that approach, we obtain expressions for electron emitted transition amplitudes from two different molecular centers, and accelerated then in the strong laser field. In addition, our approach directly underpins different underlying physical processes that correspond to (i) direct tunneling ionization; (ii) electron rescattering on the center of origin; and, finally, (iii) electron rescattering on a different center. One innovative aspect of our theory is the fact that the dipole matrix elements are free from nonphysical gauge and coordinate system-dependent terms: this is achieved by adapting the coordinate system, in which SFA is performed, to the center from which the corresponding part of the time-dependent wave function originates. Our analytic results agree very well with the numerical solution of the full three-dimensional TDSE for the  $\text{H}_2^+$  molecule. Moreover, the theoretical model was applied to describe laser-induced electron diffraction measurements of  $\text{O}_2^+$  molecules, obtained at ICFO, and reproduces the main features of the experiment very well. Our approach can be extended in a natural way to more complex molecules and multielectron systems.

DOI: [10.1103/PhysRevA.94.043423](https://doi.org/10.1103/PhysRevA.94.043423)**I. INTRODUCTION****A. Imaging in strong fields: High-order harmonic generation and laser-induced electron diffraction**

One of the most exciting prospects of strong-field and attosecond physics is the extraction of electronic and nuclear information on the attosecond temporal and picometer spatial scales [1]. Strong-field techniques such as high harmonic spectroscopy (HHS) [2–4] exploit the quiver motion of an electron which is liberated from the target structure itself and analyze either the recombination spectrum or the momentum distribution of the rescattering electron [5–7].

In a seminal work, Villeneuve *et al.* [8] demonstrated that a tomographic reconstruction from a HHS measurement yields the Dyson orbital of  $\text{N}_2$  [9]. The original interpretation of these experiments was based on the strong-field approximation (SFA) description of the process [10], which provides a fully quantum description of the well-known “three-step model” [1,11–13]. Villeneuve *et al.*'s [8] experiment has triggered a true avalanche of experimental and theoretical works on the subject [2,14–21]. The use of approximations (and in particular the SFA) in the tomography of molecular orbitals is, however, under permanent debate and full for controversial issues: the results strongly depend on the gauge, the choice of the dipole

radiation form, the molecular orbital symmetry, and degree of alignment and the reconstruction axis (cf. [22–30]).

Laser-induced electron diffraction (LIED) [5,31,32] is based on extracting structural information directly from electrons which are elastically scattered of the parent ion. Recently, LIED has been used to successfully recover structural information from diatomic and larger polyatomic molecules [20,33–35]. An electron may directly depart from the molecule and contribute to the lower-energy region of the above-threshold ionization (ATI) spectrum; this process is termed direct tunneling or it might return to the target molecular ion, driven by the still present laser electric field, and rescatter, thereby gaining much more energy. This high energetic electron could excite the remaining ion or even cause the detachment of a second electron (for a consistent description of these processes within the framework of the SFA and Feynman's path-integral approach, see [36]).

The viability of this self-imaging technique to retrieve structural information of molecular and atomic systems has been demonstrated in a series of contributions [33,34,37]. The idea is here to gain insight about the electronic structure of molecular targets interpreting the energy spectra and angular distribution of above-threshold ionization electrons. In particular, the high-energy region of the ATI spectra, which is mainly due to the rescattering process, is particularly sensitive to the structure of the target, i.e., the rescattered electron has incurred information about the target it rescattered off and hence permits extracting structural information.

\*noslen.suarez@icfo.es

Some efforts have been already made in the study and development of new theoretical tools to investigate the structure of complex systems (such as molecules, atom clusters, and solids) using the ATI spectra. Among those investigations, ATI from diatomic systems is the most widely studied process [38–41]. Two methods are commonly used and compared: a fully quantum-mechanical description based on the numerical solution of the time-dependent Schrödinger equation (TDSE) and approximated methods based on the SFA and other quasiclassical approaches. We should mention, however, that the former is only feasible for simple diatomic molecules, e.g.,  $\text{H}_2^+$ ,  $\text{H}_2$ ,  $\text{D}_2$ , and within the single active electron (SAE) approximation. The results so far focus, for instance, in the differences between the length and velocity gauge [42], the influence of the internuclear distance [40], or alignment [6,31,38,39,43] on the ATI photoelectron spectra and the importance of the residual Coulomb interaction [41,44]. While TDSE provides the most accurate description of the underlying physics behind LIED, it is numerically and computationally very costly. In addition, the multidimensional TDSE can currently not be solved for complex molecules, multielectron systems, or molecular systems evolving in time. Thus, one has to resort to approximate descriptions such as the SFA and related methods to adequately describe the more complex instances of LIED. Similar arguments can be put forward for molecular orbital tomography methods based on high-order harmonic generation (HHG).

### B. Overcoming the drawbacks of SFA

The standard SFA method, however, has severe drawbacks, namely, the electronic states in the continuum are described in their simplest approximation by Volkov states (a plane wave in the presence of the laser field) or, in a slightly more sophisticated version, by Coulomb-Volkov states or similar ones which take into account Coulomb corrections [45–47]. These states are typically not orthogonal to the target bound states and this introduces spurious contributions. For instance, when we compute the transition dipole matrix element  $\mathbf{d}(\mathbf{v})$  between the bound  $|0\rangle$  and continuum  $|\phi_{\mathbf{v}}\rangle$  states, the results depend linearly on the choice of the center of the coordinate system:  $\mathbf{d}(\mathbf{v}) = q_e \langle \phi_{\mathbf{v}} | \hat{\mathbf{r}} | 0 \rangle \neq q_e \langle \phi_{\mathbf{v}} | (\hat{\mathbf{r}} - \mathbf{R}) | 0 \rangle$ , where  $\mathbf{R}$  is a constant coordinate shift, typically corresponding to the distance between the nuclei (the so-called internuclear distance) in a two-center molecule. This is an artificial and nonphysical effect, particularly problematic when  $\mathbf{R} \rightarrow \infty$ . Most authors handle this problem by neglecting the linear terms in  $\mathbf{R}$  in the dipole matrix elements [40,42,43]. Nevertheless, this is not a systematic approach since it does not solve adequately problems related with various phase factors appearing on the molecular dipole matrix elements. In addition, they present a strong dependence on the choice of the gauge, or complications with the correct asymptotic behavior for  $\mathbf{R} \rightarrow \infty$  and yet to  $\mathbf{R} \rightarrow 0$  (cf. [40]). Furthermore, the agreement with the TDSE results is typically poor. Aside from the mentioned weaknesses, we should note that these previous studies have led to a relatively good description of the ATI process in diatomic molecules.

In this paper, we propose a natural and systematic solution of all the above-mentioned problems by extending the SFA

to complex molecules without ambiguities. Our version of the SFA for ATI and HHG has the following appealing properties:

(a) It analytically reproduces the results for  $\mathbf{R} \rightarrow \infty$ ; for the particular case of diatomic molecules, this corresponds to two identical atoms (sources) generating electronic (photonic) states with a phase difference corresponding to the distance  $\mathbf{R}$  between them.

(b) It reproduces analytically the asymptotic limit for  $\mathbf{R} \rightarrow 0$ ; for the case of a diatomic molecule, we end up with the usual single-atom formulation.

(c) Statements (a) and (b) agree well with their counterpart solutions obtained using the three-dimensional TDSE (3D-TDSE).

(d) It allows us to interpret the results in terms of quantum orbits, e.g., we could disentangle contributions for electrons originating at a given center  $\mathbf{R}_i$  that rescatters at another one  $\mathbf{R}_j$ , etc.

(e) It is free of nonphysical dependencies on  $\mathbf{R}_i$ .

(f) It agrees well with experimental results at ICFO concerning  $\text{O}_2^+$  molecules.

Our approach is based on the following observation: both in the ATI and HHG cases the molecular response, which is determined by the probability amplitude of an electron in the continuum with a given energy and velocity, depends linearly on the wave functions of the initial (ground) state. More generally, the solution of the *linear* TDSE depends *linearly* on the wave function of the initial state. Commonly, for a molecule it is natural to write this function as a summation of the contributions corresponding to different nuclei: for a diatomic molecule it is a sum of two terms, for triatomic molecules a sum of three, etc. Following this reasoning, our modified SFA consists in the following steps:

(i) Decompose the initial ground state of the molecule into a superposition of terms centered at  $\mathbf{R}_i$ ,  $i = 1, 2, \dots$ , i.e., at the position where the heavy nuclei are located.

(ii) Solve independently a TDSE, exactly or using the SFA for each term, using a coordinate system centered at each  $\mathbf{R}_i$ .

(iii) Transform at the end all terms to the same coordinate system and coherently add them up.

Further, this approach is formally exact, as the exact numerical solutions of the TDSE are used; in fact it might even have some numerical advantages. On the other hand, the formulation is approximated if the SFA is used to solve the TDSE, but this approach seems to give particularly robust outcomes which agreed very well with the exact ones.

We illustrate our point with the simplest possible example: a two-center molecule with two identical atoms separated at certain distance  $R$  driven by a strong ultrashort laser field linearly polarized along the  $z$  direction, but nothing prevents to apply our formalism to more complex molecular targets. To model the electron-heavy ion interactions we take advantage of the short-range potential model developed by Becker *et al.* [48]. Considering the ATI spectra are sensitive to the internuclear distance and the orientation between the molecular axis and the polarization direction of the laser field  $z$ , we aim to generalize the SFA for atomic systems presented in [49,50] to the above-mentioned diatomic molecular targets. Furthermore, we put particular emphasis to all the possible scenarios: tunneling ionization from both centers and propagation in the continuum until the measurement process; tunneling ionization from one

particular center, electron propagation in the continuum, and rescattering on the same parent center; tunneling ionization from one center, electron propagation in the continuum, and rescattering with its neighboring parent center; and (perhaps the most peculiar one) tunneling ionization from one center, electron propagation in the continuum, and rescattering on the same center, causing electron rescattering from the parent neighboring center.

We stress, in the end, that the agreement of our results with the TDSE solution is remarkably good, which allows us to seriously think in extensions of our SFA version to tackle more complex molecules, with three or more molecular centers, and systems with more active electrons, where the solution of the exact Schrödinger equation is not currently available.

### C. Plan of the paper

This article is organized as follows. In Sec. II, we write the formulas for the two-center molecular system ATI transition amplitude, for both the direct and rescattered electrons, using the prescriptions presented above. In Sec. III, we introduce a particular nonlocal short-range (SR) model potential to calculate the bound and rescattering electron states. The matrix elements that describe the ionization and rescattering processes are then provided in an analytic form. We use them in Sec. IV to compute both energy-resolved ATI and two-dimensional electron momentum distributions for a diatomic molecule. Here, our numerical results are compared with numerical results obtained from TDSE calculations. The basic analysis of the interference minima of the photoelectron spectra and the discussion of how structural information, the internuclear distance, could be retrieved is presented in this section. In Sec. V, we confront and compare our results with experimental results obtained at ICFO for  $O_2^+$  molecules. Clearly, the comparison is very encouraging and suggests that our theory is on the right track to describe experiments in more complex systems. Finally, in Sec. VI, we summarize the main ideas and present our conclusions.

## II. GENERALIZED STRONG-FIELD APPROXIMATION: TRANSITION PROBABILITY AMPLITUDES

### A. Basics of SFA: A remainder

We aim to extend the SFA from atomic systems presented Ref. [50] to molecular targets. In particular, we focus ourselves on calculating the final photoelectron spectrum by means of solving the TDSE for a molecule with two identical centers separated by a distance  $R$  and driven by a short and intense linearly polarized laser pulse. We define the relative vector position  $\mathbf{R} = \mathbf{R}_2 - \mathbf{R}_1$  where  $\mathbf{R}_1 = -\frac{\mathbf{R}}{2}$  ( $\mathbf{R}_2 = +\frac{\mathbf{R}}{2}$ ) is the position of one atom placed at the *left* (*right*). In general, as the molecular nuclei are much heavier than the electrons and the laser pulse duration is shorter than the nuclei vibration and rotational dynamics, we fix the nuclei positions and neglect the repulsive interaction between them. Further, throughout the formulation we consider the so-called single active electron (SAE) approximation.

The TDSE that describes the whole laser-molecule interactions (atomic units are used throughout this paper unless

otherwise stated) can be written as

$$i \frac{\partial}{\partial t} |\Psi(t)\rangle = \hat{H} |\Psi(t)\rangle = [\hat{H}_0 + \hat{V}_{int}(\mathbf{r}, t)] |\Psi(t)\rangle, \quad (1)$$

where  $\hat{H}_0 = \frac{\hat{\mathbf{p}}^2}{2} + \hat{V}(\mathbf{r})$  defines the laser-field free Hamiltonian, with  $\hat{\mathbf{p}} = -i\nabla$  the canonical momentum operator and  $\hat{V}(\mathbf{r})$  potential operator that describes the interaction of the nuclei with the active electron and  $\hat{V}_{int}(\mathbf{r}, t) = -q_e \hat{\mathbf{E}}(t) \cdot \hat{\mathbf{r}}$  represents the interaction of the molecular system with the laser radiation, written in the dipole approximation and length gauge.  $q_e$  denotes the electron charge which in atomic units has the value of  $q_e = -1.0$  a.u. Finally, the linearly polarized, in the  $z$  axis, laser electric field has the form  $\mathbf{E}(t) = \mathcal{E}_0 f(t) \sin(\omega_0 t + \phi_0) \mathbf{e}_z$ , where  $\mathcal{E}_0$ ,  $\omega_0$ ,  $f(t)$ , and  $\phi_0$  are the electric field peak amplitude, the carrier frequency, the laser envelope, and the carrier-envelope phase (CEP), respectively. We have defined the laser pulse envelope as  $f(t) = \sin^2(\frac{\omega_0 t}{2N_c})$  where  $N_c$  is the number of total cycles.

We shall restrict our model to the low ionization regime, where the SFA is valid [10,49,51–54]. Therefore, we work in the tunneling regime, where the Keldysh parameter  $\gamma = \sqrt{I_p/2U_p}$  ( $I_p$  is the ionization potential of the system and  $U_p = \frac{\mathcal{E}_0^2}{4\omega_0^2}$  the ponderomotive energy acquired by the electron during its incursion in the field) is less than one, i.e.,  $\gamma < 1$ . In addition, we assume that  $V(\mathbf{r})$  does not play an important role in the electron dynamics once the electron appears in the continuum.

These observations, and the following three statements, define the standard SFA, namely,

- (i) only the ground state  $|0\rangle$  and the continuum states  $|\mathbf{v}\rangle$  are taken into account in the interaction process;
- (ii) there is no depletion of the ground state ( $U_p < U_{sat}$ );
- (iii) the continuum states are approximated by Volkov states; in the continuum the electron is considered as a free particle solely moving in the laser electric field.

For a more detailed discussion of the validity of the above statements, see, e.g., Refs. [10,49,50].

### B. SFA: An appropriate treatment of two-center systems

Based on the statement (i) and the linearity of the Schrödinger equation, we propose a general state for the system:

$$|\Psi(t)\rangle = |\Psi_{\mathcal{L}}(t)\rangle + |\Psi_{\mathcal{R}}(t)\rangle, \quad (2)$$

which is the coherent superposition of two states  $|\Psi_{\mathcal{L}}(t)\rangle$  and  $|\Psi_{\mathcal{R}}(t)\rangle$ . The subindices “ $\mathcal{L}$ ” and “ $\mathcal{R}$ ” refer to the contributions of the spatially localized *left* and *right* nuclei, respectively. We note that those *left-right* states are not orthogonal between them. Following the same assumption as that in our previous contribution [49,50], each single state can be written as the coherent superposition of ground *left-right* and continuum states

$$|\Psi_{\mathcal{L}}(t)\rangle = e^{iI_p t} \left[ a(t) |0_{\mathcal{L}}\rangle + \int d^3\mathbf{v} b_{\mathcal{L}}(\mathbf{v}, t) |\mathbf{v}\rangle \right], \quad (3)$$

$$|\Psi_{\mathcal{R}}(t)\rangle = e^{iI_p t} \left[ a(t) |0_{\mathcal{R}}\rangle + \int d^3\mathbf{v} b_{\mathcal{R}}(\mathbf{v}, t) |\mathbf{v}\rangle \right]. \quad (4)$$

Note that the whole ground state, i.e.,  $|0\rangle = |0_{\mathcal{L}}\rangle + |0_{\mathcal{R}}\rangle$ , is a composition of *left*  $|0_{\mathcal{L}}\rangle$  and *right*  $|0_{\mathcal{R}}\rangle$  contributions. In this way, we are able to separate the whole state  $|\Psi(t)\rangle$  both as the *left-right* states described in Eq. (2) and the two above ones [Eqs. (3) and (4)].

The factor  $a(t)$  represents the amplitude of the state  $|0\rangle$  and it is considered constant in time  $a(t) \approx 1$  under the assumptions of the statement (ii). The prefactor  $e^{iI_p t}$  describes the accumulated electron energy in the ground state where  $I_p = -E_0$  ( $E_0$  is the molecular ground-state energy). Furthermore, the continuum states transition amplitudes  $b_{\mathcal{L}}(\mathbf{v}, t)$  and  $b_{\mathcal{R}}(\mathbf{v}, t)$  are referring to the electron wave function ionized from the *left* and *right* nuclei, respectively.

Our main task will be thereby to derive general expressions, by means of the Eq. (1) and the definitions of Eqs. (3) and (4), for the transition amplitudes  $b_{\mathcal{L}}(\mathbf{v}, t)$  and  $b_{\mathcal{R}}(\mathbf{v}, t)$ . We shall consider that  $\hat{H}_0|0_{\mathcal{L},\mathcal{R}}\rangle = -I_p|0_{\mathcal{L},\mathcal{R}}\rangle$  and  $\hat{H}_0|\mathbf{v}\rangle = \frac{v^2}{2}|\mathbf{v}\rangle$  fulfill for the bound and continuum states, respectively. Consequently, the evolution of the transition amplitude  $b_{\mathcal{L}}(\mathbf{v}, t)$  becomes

$$\begin{aligned} & i \int d^3\mathbf{v} \dot{b}_{\mathcal{L}}(\mathbf{v}, t) |\mathbf{v}\rangle \\ &= \int d^3\mathbf{v} \left( \frac{v^2}{2} + I_p \right) b_{\mathcal{L}}(\mathbf{v}, t) |\mathbf{v}\rangle + \mathbf{E}(t) \cdot \mathbf{r} |0_{\mathcal{L}}\rangle \\ & \quad + \mathbf{E}(t) \cdot \mathbf{r} \int d^3\mathbf{v} b_{\mathcal{L}}(\mathbf{v}, t) |\mathbf{v}\rangle. \end{aligned} \quad (5)$$

On the above equation we have assumed that the electron-nuclei interactions are neglected once the electron appears in the continuum, based on the statement (iii). Therefore, by multiplying Eq. (5) by  $\langle \mathbf{v}' |$  and after some algebra, the time variation of the transition amplitude reads as

$$\begin{aligned} \dot{b}_{\mathcal{L}}(\mathbf{v}, t) &= -i \left( \frac{v^2}{2} + I_p \right) b_{\mathcal{L}}(\mathbf{v}, t) + i \mathbf{E}(t) \cdot \mathbf{d}_{\mathcal{L}}(\mathbf{v}) \\ & \quad - i \mathbf{E}(t) \cdot \int d^3\mathbf{v}' b_{\mathcal{L}}(\mathbf{v}', t) \langle \mathbf{v} | \mathbf{r} | \mathbf{v}' \rangle. \end{aligned} \quad (6)$$

The first two terms on the right-hand side of Eq. (6) represent the phase evolution of the electron within the oscillating laser field. In the last term, we have defined the bound-free transition dipole matrix element as

$$\mathbf{d}_{\mathcal{L}}(\mathbf{v}) = -\langle \mathbf{v} | \mathbf{r} | 0_{\mathcal{L}} \rangle. \quad (7)$$

Here,  $|\mathbf{v}\rangle$  represents in general a scattering state built up as the superposition of a plane wave  $|\mathbf{v}_p\rangle$  and corrections on the *left*  $|\delta\mathbf{v}_{\mathcal{L}}\rangle$  and on the *right*  $|\delta\mathbf{v}_{\mathcal{R}}\rangle$ :

$$|\mathbf{v}\rangle = |\mathbf{v}_p\rangle + |\delta\mathbf{v}_{\mathcal{L}}\rangle + |\delta\mathbf{v}_{\mathcal{R}}\rangle. \quad (8)$$

Based on statement (iii), our formulation only considers the continuum state as a plane wave  $|\mathbf{v}_p\rangle$  for the calculation of the bound-free dipole matrix element. We shall pay special attention to the computation of Eq. (7). Let us stress the fact that plane waves are not orthogonal to the bound states. Notice also that our bound state is defined depending on the relative position of one of the atoms  $\mathbf{R}_1$  with respect to the origin of coordinates. In this sense, we need to introduce a ‘‘position correction’’ on the dipole transition matrix in order to avoid nonphysical terms with linear dependence on  $\mathbf{R}$  (see Sec. I B

for more details). So, for the *left* contribution we introduce a correction to the dipole matrix element as

$$\begin{aligned} \mathbf{d}_{\mathcal{L}}(\mathbf{v}) &= -\langle \mathbf{v}_p | (\mathbf{r} - \mathbf{R}_1) | 0_{\mathcal{L}} \rangle \\ &= -\langle \mathbf{v}_p | \mathbf{r} | 0_{\mathcal{L}} \rangle + \mathbf{R}_1 \langle \mathbf{v}_p | 0_{\mathcal{L}} \rangle. \end{aligned} \quad (9)$$

Similarly for  $b_{\mathcal{R}}(\mathbf{v}, t)$  we define a bound-free transition dipole matrix  $\mathbf{d}_{\mathcal{R}}(\mathbf{v}) = -\langle \mathbf{v}_p | (\mathbf{r} - \mathbf{R}_2) | 0_{\mathcal{R}} \rangle$ , and the total bound-free transition dipole matrix is thus  $\mathbf{d}_m(\mathbf{v}) = \mathbf{d}_{\mathcal{L}}(\mathbf{v}) + \mathbf{d}_{\mathcal{R}}(\mathbf{v})$ . For atomic systems, the above analysis is not necessary since the atom is placed at the origin of the coordinate system. Furthermore, in the second term of Eq. (9) the continuum state  $|\mathbf{v}\rangle$  is an eigenstate of the full atomic Hamiltonian  $H_0$ , therefore, this extra term  $\mathbf{R}_1 \langle \mathbf{v}_p | 0_{\mathcal{L}} \rangle$  disappears.

On the third term of Eq. (6), we define the continuum-continuum transition matrix element  $\mathbf{G}_m(\mathbf{v}, \mathbf{v}') = \langle \mathbf{v} | \mathbf{r} | \mathbf{v}' \rangle$  that relies upon on the scattering states  $|\mathbf{v}\rangle$  and  $|\mathbf{v}'\rangle$  defined in Eq. (8) as

$$\mathbf{G}_m(\mathbf{v}, \mathbf{v}') = i \nabla_{\mathbf{v}} \delta(\mathbf{v} - \mathbf{v}') - \mathbf{R}_1 \delta(\mathbf{v} - \mathbf{v}') + \mathbf{g}_m(\mathbf{v}, \mathbf{v}'). \quad (10)$$

The first two terms on the right-hand side of Eq. (10) describe the motion of a free electron in the continuum. They are associated to events where the laser-ionized electron is accelerated by the laser electric field without any probability of rescattering. The last one, the rescattering transition matrix element  $\mathbf{g}_m(\mathbf{v}, \mathbf{v}')$ , accounts for all the rescattering processes concerning the entire molecule. For  $\mathbf{g}_m(\mathbf{v}, \mathbf{v}')$  the residual Coulomb potential has to be taken into account. In this sense, it can be written as a sum of components representing each rescattering channel on the molecule. The third term of Eq. (10) then reads as

$$\begin{aligned} \mathbf{g}_m(\mathbf{v}, \mathbf{v}') &= \mathbf{g}_{\mathcal{L}\mathcal{L}}(\mathbf{v}, \mathbf{v}') + \mathbf{g}_{\mathcal{R}\mathcal{R}}(\mathbf{v}, \mathbf{v}') + \mathbf{g}_{\mathcal{R}\mathcal{L}}(\mathbf{v}, \mathbf{v}') + \mathbf{g}_{\mathcal{L}\mathcal{R}}(\mathbf{v}, \mathbf{v}') \\ &= \langle \mathbf{v}_p | (\mathbf{r} - \mathbf{R}_1) | \delta\mathbf{v}'_{\mathcal{L}} \rangle + \langle \delta\mathbf{v}_{\mathcal{R}} | (\mathbf{r} - \mathbf{R}_2) | \mathbf{v}'_p \rangle \\ & \quad + \langle \delta\mathbf{v}_{\mathcal{L}} | (\mathbf{r} - \mathbf{R}_1) | \mathbf{v}'_p \rangle + \langle \mathbf{v}_p | (\mathbf{r} - \mathbf{R}_2) | \delta\mathbf{v}'_{\mathcal{R}} \rangle. \end{aligned} \quad (11)$$

The first two terms in the above equation contain information about spatially local processes involving only one of the atoms: the so-called local terms. On the contrary, the last two ones, describe processes involving both atomic centers, henceforth, we refer to them as nonlocal and cross terms, respectively.

Next, we include corrections on Eq. (6), extending the analysis based on the orthogonality of the plane and rescattering waves, discussed before. The transition amplitude for the *left* states then reads as

$$\begin{aligned} \dot{b}_{\mathcal{L}}(\mathbf{v}, t) &= -i \left[ \frac{v^2}{2} + I_p - \mathbf{R}_1 \cdot \mathbf{E}(t) \right] b_{\mathcal{L}}(\mathbf{v}, t) + i \mathbf{E}(t) \cdot \mathbf{d}_{\mathcal{L}}(\mathbf{v}) \\ & \quad + \mathbf{E}(t) \cdot \nabla_{\mathbf{v}} b_{\mathcal{L}}(\mathbf{v}, t) - i \mathbf{E}(t) \cdot \\ & \quad \times \int d^3\mathbf{v}' b_{\mathcal{L}}(\mathbf{v}', t) \mathbf{g}_m(\mathbf{v}, \mathbf{v}'). \end{aligned} \quad (12)$$

The transition amplitude for the *right* states can be found following exactly the same procedure, namely, (i) projecting the entire Hamiltonian of the system on the *right* wave function (4) to get an equation similar to Eq. (5); (ii) multiplying it by a scattering state  $\langle \mathbf{v}' |$ , and (iii) defining the bound-continuum and continuum-continuum transition matrix elements including their respective corrections.

A general equation containing both of the processes mentioned before reads as

$$\begin{aligned} \dot{b}_j(\mathbf{v}, t) = & -i \left[ \frac{\mathbf{v}^2}{2} + I_p - \mathbf{R}_i \cdot \mathbf{E}(t) \right] b_j(\mathbf{v}, t) \\ & + i \mathbf{E}(t) \cdot \mathbf{d}_j(\mathbf{v}) + \mathbf{E}(t) \cdot \nabla_{\mathbf{v}} b_j(\mathbf{v}, t) \\ & - i \mathbf{E}(t) \cdot \int d^3 \mathbf{v}' b_j(\mathbf{v}', t) \mathbf{g}_m(\mathbf{v}, \mathbf{v}'), \end{aligned} \quad (13)$$

where the subscript  $j$  represents either the *left*  $j = \mathcal{L}$  or *right*  $j = \mathcal{R}$  and  $i = 1, 2$  is the position of the atom. For instance, to obtain the transition amplitude for the *left* states [Eq. (12)], we need to set  $j = \mathcal{L}$  and  $i = 1$  in the above equation.

In the following, we shall describe how it is possible to compute the transition amplitude  $b_j(\mathbf{v}, t)$  by applying the zeroth- and first-order perturbation theories to the solution of the partial differential equation (13). According to the perturbation theory, the transition amplitude solution  $b_j(\mathbf{v}, t)$  can be split into two parts:  $b_{0,j}(\mathbf{v}, t)$  and  $b_{1,j}(\mathbf{v}, t)$ , i.e.,  $b_j(\mathbf{v}, t) = b_{0,j}(\mathbf{v}, t) + b_{1,j}(\mathbf{v}, t)$ , the zeroth-order solution  $b_{0,j}(\mathbf{v}, t)$ , and the first-perturbative-order solution  $b_{1,j}(\mathbf{v}, t)$ . These correspond to the direct and rescattering terms, respectively. As is known, the direct term describes the transition amplitude for a laser-ionized electron that never rescatters with the remaining molecular ions. On the other hand, the rescattering term  $b_{1,j}(\mathbf{v}, t)$  is referred to an electron that, once ionized in a particular center, has a certain probability of rescattering with each of the molecular ions.

### C. Direct transition amplitude

Let us consider the process where the electron is ionized from one of the atoms without probability to return to its parent ion. The last two terms in Eq. (13) describe the continuum-continuum transition  $\nabla_{\mathbf{v}} b_j(\mathbf{v}, t)$  without the influence of the scattering center, and  $\int d^3 \mathbf{v}' b_j(\mathbf{v}', t) \mathbf{g}_m(\mathbf{v}, \mathbf{v}')$  by considering the core potential. Here,  $\mathbf{g}_m(\mathbf{v}, \mathbf{v}')$  denotes the rescattering transition matrix element, where the potential core plays an essential role.

As the direct ionization process should have a larger probability compared with the rescattering one [49,50], one might neglect the last term in Eq. (13),  $\mathbf{g}_m(\mathbf{v}, \mathbf{v}') = \mathbf{0}$ . This is what we refer as zeroth-order solution:

$$\begin{aligned} \partial_t b_{0,j}(\mathbf{v}, t) = & -i \left[ \frac{\mathbf{v}^2}{2} + I_p - \mathbf{R}_i \cdot \mathbf{E}(t) \right] b_{0,j}(\mathbf{v}, t) \\ & + i \mathbf{E}(t) \cdot \mathbf{d}_j(\mathbf{v}) + \mathbf{E}(t) \cdot \nabla_{\mathbf{v}} b_{0,j}(\mathbf{v}, t). \end{aligned} \quad (14)$$

The latter equation is easily solved by conventional integration methods (see, e.g., [55]) and considering the Keldysh transformation [51,56]. Therefore, the solution is as follows:

$$\begin{aligned} b_{0,j}(\mathbf{p}, t) = & i \int_0^t dt' \mathbf{E}(t') \cdot \mathbf{d}_j[\mathbf{p} + \mathbf{A}(t')] \\ & \times \exp \left( -i \int_{t'}^t d\tilde{t} \{ [\mathbf{p} + \mathbf{A}(\tilde{t})]^2 / 2 \right. \\ & \left. + I_p - \mathbf{R}_i \cdot \mathbf{E}(\tilde{t}) \right). \end{aligned} \quad (15)$$

Note that the above equation is written in terms of the canonical momentum  $\mathbf{p} = \mathbf{v} - \mathbf{A}(t)$  [10]. Here, we have considered that

the electron appears in the continuum with kinetic momentum  $\mathbf{v}(t') = \mathbf{v} - \mathbf{A}(t) + \mathbf{A}(t')$  at the time  $t'$ , where  $\mathbf{v}$  is the final kinetic momentum (note that in atomic units  $\mathbf{p} = \mathbf{v}$ ), and  $\mathbf{A}(t) = -\int^t \mathbf{E}(t') dt'$  is the associated vector potential.

Equation (15) has a direct physical interpretation which is understood as the sum of all the ionization events that occur from the time  $t'$  to  $t$ . Then, the instantaneous transition probability amplitude of an electron at a time  $t'$ , at which it appears into the continuum with momentum  $\mathbf{v}(t') = \mathbf{p} + \mathbf{A}(t')$ , is defined by the argument of the  $[0, t]$  integral in Eq. (15). Furthermore, the exponent phase factor denotes the ‘‘semiclassical action’’  $S_i(\mathbf{p}, t, t')$ , that defines a possible electron trajectory from the birth time  $t'$ , at position  $\mathbf{R}_i$ , until the ‘‘detection’’ one  $t$  as

$$S_i(\mathbf{p}, t, t') = \int_{t'}^t d\tilde{t} \{ [\mathbf{p} + \mathbf{A}(\tilde{t})]^2 / 2 + I_p - \mathbf{R}_i \cdot \mathbf{E}(\tilde{t}) \}. \quad (16)$$

Note that the transition amplitude equations obtained so far depend on the position from which the electron is tunnel ionized to the continuum. The semiclassical action  $S_i(\mathbf{p}, t, t')$  contains this dependency as well.

Considering we are interested to obtain the transition amplitude  $b_{0,j}(\mathbf{p}, t)$  at the end of the laser pulse, the time  $t$  is set at  $t = t_F$ . Consequently, we shall define the integration time window as  $t \in [0, t_F]$ . Furthermore, we set  $\mathbf{E}(0) = \mathbf{E}(t_F) = \mathbf{0}$ , in such a way to make sure that the laser electric field is a time oscillating wave and does not contain static components [the same arguments apply to the vector potential  $\mathbf{A}(t)$ ]. Finally, the total transition amplitude for the direct process taking place on our two-center molecular system reads as

$$b_0(\mathbf{p}, t) = b_{0,\mathcal{L}}(\mathbf{p}, t) + b_{0,\mathcal{R}}(\mathbf{p}, t). \quad (17)$$

### D. Rescattering transition amplitude

In order to find the solution for the transition amplitude of the rescattered photoelectrons  $b_1(\mathbf{v}, t)$ , we have considered, in Eq. (13),  $\mathbf{g}_m(\mathbf{v}, \mathbf{v}') \neq \mathbf{0}$ . The first-order solution  $b_1(\mathbf{v}, t)$  is then obtained by inserting the zeroth-order solution  $b_{0,j}(\mathbf{p}, t)$  in the right-hand side of Eq. (13). Thereby we obtain a general equation to describe the rescattering process as

$$\begin{aligned} \dot{b}_{1,jj'}(\mathbf{v}, t) = & -i \left[ \frac{\mathbf{v}^2}{2} + I_p - \mathbf{R}_i \cdot \mathbf{E}(t) \right] b_{1,jj'}(\mathbf{v}, t) - i \mathbf{E}(t) \\ & \cdot \int d^3 \mathbf{v}' b_{0,j}(\mathbf{v}', t) \mathbf{g}_{jj'}(\mathbf{v}, \mathbf{v}'), \end{aligned} \quad (18)$$

where  $j$  denotes the atom from where the electron is released and  $j'$  the one where the electron is rescattered. As the continuum-continuum rescattering matrix element is split in four terms [see Eq. (12)], the associated rescattering transition amplitude contains four terms as well, i.e.,

$$b_1(\mathbf{v}, t) = b_{1,\mathcal{L}\mathcal{L}}(\mathbf{v}, t) + b_{1,\mathcal{L}\mathcal{R}}(\mathbf{v}, t) + b_{1,\mathcal{R}\mathcal{R}}(\mathbf{v}, t) + b_{1,\mathcal{R}\mathcal{L}}(\mathbf{v}, t). \quad (19)$$

The above equation contains information about all the possible rescattering scenarios which take place in our molecular system. In addition, a direct physical interpretation of each term can be inferred as following:

(1) The first term,  $b_{1,\mathcal{L}\mathcal{L}}(\mathbf{v}, t)$ , denotes electron-tunneling ionization from an atom located at  $\mathbf{R}_1$  and rescattering with the

same parent ion. We refer this process as “spatially localized” since the electron performs a local rescattering with the same atomic core  $j = j'$  from which it was born.

(2) The process described by  $b_{1,\mathcal{LR}}(\mathbf{v},t)$  considers both atoms of the molecule. It represents an event where the electron is tunnel ionized from an atom at  $\mathbf{R}_1$  and rescatters with the other atom at  $\mathbf{R}_2$ . We call this process as “cross process.” In fact, there exists another process involving both atoms. It occurs when the electron is detached from an atom located at  $\mathbf{R}_1$  and rescatters with the same parent ion, but there is certain probability of electron emission from the other ion core, placed at  $\mathbf{R}_2$ . We label the latter as “nonlocal process.”

(3) The other “local” term,  $b_{1,\mathcal{RR}}(\mathbf{v},t)$ , describes the same process as (1), but now for an atom located at  $\mathbf{R}_2$ .

(4) Finally,  $b_{1,\mathcal{RL}}(\mathbf{v},t)$  represents the same process as in (2), but the tunnel-ionization process takes place at  $\mathbf{R}_2$ .

The differential equation describing the local-rescattering processes is constructed considering  $j = j'$ . For processes localized at *left* we need to set  $j = j' = \mathcal{L}$  and  $i = 1$  and for the ones at the *right*  $j = j' = \mathcal{R}$  and  $i = 2$ , respectively. In this way, the transition amplitude for the local processes reads as

$$\begin{aligned} b_{1,jj}(\mathbf{p},t) = & - \int_0^t dt' \int_0^{t'} dt'' \int d^3\mathbf{p}' \mathbf{E}(t') \\ & \times \mathbf{g}_{jj}[\mathbf{p} + \mathbf{A}(t'), \mathbf{p}' + \mathbf{A}(t')] \exp[-iS_i(\mathbf{p},t,t')] \\ & \times \mathbf{E}(t'') \cdot \mathbf{d}_j[\mathbf{p}' + \mathbf{A}(t'')] \exp[-iS_i(\mathbf{p}',t',t'')]. \end{aligned} \quad (20)$$

As we expect, the rescattering transition amplitude contains two exponential factors, each representing the excursion of the electron in the continuum: before and after the rescattering event. In the above equation, both phase factors need to be evaluated with the same subscript, i.e.,  $S_1(\mathbf{p},t,t') - S_1(\mathbf{p}',t',t'')$  or  $S_2(\mathbf{p},t,t') - S_2(\mathbf{p}',t',t'')$  since they are local processes.

The last factor in Eq. (20),  $\exp[-iS_i(\mathbf{p}',t',t'')]$ , represents the accumulated phase of an electron born at the time  $t''$  in  $\mathbf{R}_i$  until it rescatters at time  $t'$ . In the same way  $\exp[-iS_i(\mathbf{p},t,t')]$  defines the accumulated phase of the electron after it rescatters at a time  $t'$  to the “final” one  $t$ , when the electron is “measured” at the detector with momentum  $\mathbf{p}$ . Finally, the quantity  $\mathbf{E}(t'') \cdot \mathbf{d}_j[\mathbf{p}' + \mathbf{A}(t'')]$  is the probability amplitude of an emitted electron at the time  $t''$  that has a kinetic momentum of  $\mathbf{v}'(t'') = \mathbf{p}' + \mathbf{A}(t'')$ . Similarly, to find the transition amplitude for a local process at the *right* atom, we need to consider  $j = j' = \mathcal{R}$  and  $i = 2$  in Eq. (20) and use the *right* dipole transition matrix element.

The cross and nonlocal processes are formulated by considering  $j \neq j'$  in the following way:  $j = \mathcal{L}, \mathcal{R}, j' = \mathcal{R}, \mathcal{L}$  in Eq. (18). The phase factors have to be set in different atomic positions: it means  $S_1(\mathbf{p},t,t') - S_2(\mathbf{p}',t',t'')$  or  $S_2(\mathbf{p},t,t') - S_1(\mathbf{p}',t',t'')$ . For instance, the transition amplitude for the *left-right* reads as

$$\begin{aligned} b_{1,\mathcal{LR}}(\mathbf{p},t) = & - \int_0^t dt' \int_0^{t'} dt'' \int d^3\mathbf{p}' \mathbf{E}(t') \\ & \times \mathbf{g}_{\mathcal{LR}}[\mathbf{p} + \mathbf{A}(t'), \mathbf{p}' + \mathbf{A}(t')] \exp[-iS_2(\mathbf{p},t,t')] \\ & \times \mathbf{E}(t'') \cdot \mathbf{d}_{\mathcal{L}}[\mathbf{p}' + \mathbf{A}(t'')] \exp[-iS_1(\mathbf{p}',t',t'')]. \end{aligned} \quad (21)$$

Here, we notice that the above equation describes the atomic system presented in Ref. [50] when the internuclear distance goes to zero,  $\mathbf{R} \rightarrow 0$ . The verification of this limit for the direct process is straightforward. The phase factor in Eq. (16) then becomes the well-known semiclassical action  $S(\mathbf{p},t,t')$  and the transition amplitude exactly has the same dependency as for an atom, if we replace the atomic matrix elements on it. For the rescattering events, we have to neglect in Eq. (19) the contribution of the nonlocal and cross terms (the last two terms) and follow the same procedure as before. In the following sections, we obtain the exact dependency of the rescattered matrix elements and demonstrate that the atomic limit can also be recovered when  $\mathbf{R} \rightarrow 0$ .

In the total rescattering transition amplitude, Eq. (19), we can identify two main contributions, namely, one generated for the local processes and the other one for the nonlocal and cross processes. In this way, we define the rescattering transition amplitude as

$$b_1(\mathbf{p},t) = b_{\text{local}}(\mathbf{p},t) + b_{\text{nonlocal+cross}}(\mathbf{p},t), \quad (22)$$

where

$$b_{\text{local}}(\mathbf{p},t) = b_{1,\mathcal{LL}}(\mathbf{p},t) + b_{1,\mathcal{RR}}(\mathbf{p},t) \quad (23)$$

and

$$b_{\text{nonlocal+cross}}(\mathbf{p},t) = b_{1,\mathcal{LR}}(\mathbf{p},t) + b_{1,\mathcal{RL}}(\mathbf{p},t). \quad (24)$$

The total photoelectron spectra,  $|b(\mathbf{p},t_F)|^2$ , is computed as a coherent superposition of both the direct  $b_0(\mathbf{p},t_F)$  and rescattered  $b_1(\mathbf{p},t_F)$  transition amplitudes, i.e.,

$$\begin{aligned} |b(\mathbf{p},t_F)|^2 &= |b_0(\mathbf{p},t_F) + b_1(\mathbf{p},t_F)|^2 \\ &= |b_0(\mathbf{p},t_F)|^2 + |b_1(\mathbf{p},t_F)|^2 + b_0(\mathbf{p},t_F)b_1^*(\mathbf{p},t_F) + \text{c.c.} \end{aligned} \quad (25)$$

The direct transition amplitude, Eq. (15), is a “single time integral” and can be computed straightforwardly. For the rescattering one, Eqs. (20) and (21), the multiple time (“2D”) and momentum (“3D”) integrals present a demanding task from a computational perspective. In order to reduce the computational difficulties, and to obtain a physical interpretation of the ATI process, we shall employ the stationary phase method to partially evaluate these highly oscillatory integrals.

The fast oscillations of the momentum  $\mathbf{p}'$  integral suggest the utilization of the stationary-phase approximation or saddle-point method to solve it in Eq. (20). This method is expected to be accurate, when both the  $U_p$  and the  $I_p$ , as well as the involved momentum  $\mathbf{v}$  and  $\mathbf{v}'$ , are large. The quasiclassical action for the two-center molecule, Eq. (16), can be rewritten as

$$S_i(\mathbf{p}',t',t'') = \mathbf{R}_i \cdot [\mathbf{A}(t') - \mathbf{A}(t'')] + S(\mathbf{p}',t',t''), \quad (26)$$

where  $S(\mathbf{p}',t',t'') = \int_{t''}^{t'} d\tilde{t} \{[\mathbf{p}' + \mathbf{A}(\tilde{t})]^2/2 + I_p\}$  is proportional to  $I_p$ ,  $U_p$ , and  $\mathbf{p}'^2$ , and, as a consequence, the phase factor  $\exp[-iS_i(\mathbf{p}',t',t'')]$  in Eq. (20) oscillates very rapidly. Then, the integral over the momentum  $\mathbf{p}'$  of Eq. (20) tends towards zero except near the extremal points of the phase, i.e., when  $\nabla_{\mathbf{p}'} S(\mathbf{p}') = \mathbf{0}$ . Thus, the main contributions to the momentum integral are dominated by momenta  $\mathbf{p}'_s$ , which satisfy the solution of the equation  $\nabla_{\mathbf{p}'} S(\mathbf{p}')|_{\mathbf{p}'_s} = \mathbf{0}$ . These

saddle-point momenta read as

$$\mathbf{p}'_s = -\frac{1}{\tau} \int_{t''}^{t'} \mathbf{A}(\tilde{t}) d\tilde{t}. \quad (27)$$

Here,  $\tau = t' - t''$  is the excursion time of the electron in the continuum. In terms of classical mechanics, these momenta roots  $\mathbf{p}'_s$  are those corresponding to the classical electron trajectories because the momentum gradient of the action can be understood as the displacement of a particle [57]. As the momentum gradient of the action is null  $\Delta \mathbf{r} = \nabla_{\mathbf{p}'} S(\mathbf{p}', t', t'') = \mathbf{0}$ , the considered electron trajectories  $\mathbf{r}(t)$  are for an electron that is born at the time  $t''$  at a certain position  $\mathbf{r}(t'') = \mathbf{r}_0$ . Then, after some time  $t'$  the electron returns to the initial position  $\mathbf{r}(t') = \mathbf{r}_0$  with an average momentum  $\mathbf{p}'_s$ . Therefore, the function  $S(\mathbf{p}', t', t'')$  can be expanded in a Taylor series around the roots  $\mathbf{p}'_s$  and then apply the standard saddle-point method to the 3D momentum integral over  $\mathbf{p}'$  in all the rescattering equations  $b_{1,jj'}(\mathbf{p}, t)$ :

$$\begin{aligned} & \int d^3 \mathbf{p}' f(\mathbf{p}') \exp[-iS(\mathbf{p}')] \\ &= \int d^3 \mathbf{p}' f(\mathbf{p}'_s) \exp \left\{ -i \left[ S(\mathbf{p}'_s) + \frac{1}{2} \nabla_{\mathbf{p}'}^2 S(\mathbf{p}') \right]_{\mathbf{p}'_s} \right. \\ & \quad \left. \times (\mathbf{p}' - \mathbf{p}'_s)^2 \right\} \\ & \approx \left( \frac{\pi}{\varepsilon + \frac{i(t'-t'')}{2}} \right)^{\frac{3}{2}} \exp[-iS(\mathbf{p}'_s)] f(\mathbf{p}'_s). \end{aligned} \quad (28)$$

Here, we have introduced an infinitesimal parameter  $\varepsilon$  to avoid the divergence at  $t' = t''$ . Still, the singularity is not integrable and practically impossible to be treated numerically. One should stress, however, that it is the result of the saddle-point approximation restricted exclusively to the classical action. We have regarded in the calculation that the function  $f(\mathbf{p}')$  is localized at a certain scale and consequently the singularity would simply disappear. This observation and the simple method to handle it has been pioneered in Ref. [10] (for more information see the previous discussion in Ref. [50]). The simplest way to avoid the problem is to set  $\varepsilon$  small, but nonzero; throughout this paper we use  $\varepsilon = 0.4 \text{ a.u.} = 0.2/I_p$ .

With the last equation [Eq. (28)], we have substantially reduced the dimensionality of the problem, i.e., from a 5D integral to a 2D one. This reduction is extremely advantageous from a computational viewpoint. Moreover, with the saddle-point method a quasiclassical picture for the rescattering transition amplitude is obtained for molecular systems, similarly to the atomic approach described in [1,49,50].

In order to calculate the total photoelectron spectra for the two-center molecular system, we first need to define the ground and the continuum states. After having found them, we then compute the bound-free transition dipole matrix elements  $\mathbf{d}_{\mathcal{L}}(\mathbf{v})$  and  $\mathbf{d}_{\mathcal{R}}(\mathbf{v})$  and the continuum-continuum transition rescattering matrix element  $\mathbf{g}_m(\mathbf{v}, \mathbf{v}')$ . In the next section, we shall introduce a short-range potential model in order to analytically compute both the transition matrix elements and the final photoelectron momentum distribution.

### III. ABOVE-THRESHOLD IONIZATION IN DIATOMIC MOLECULES

#### A. A simplified molecular model

In this section, we define a simplified molecular model to validate the general above-described formulation and to compute the ATI photoelectron spectra. Let us consider a diatomic molecule constructed as two fixed nuclear centers under the SAE. We describe the interaction of the electron with each molecular nuclei by a nonlocal potential. The Hamiltonian  $\hat{H}(\mathbf{p}, \mathbf{p}')$  of the system in the momentum representation can be written as

$$\hat{H}_M(\mathbf{p}, \mathbf{p}') = \frac{\mathbf{p}^2}{2} \delta(\mathbf{p} - \mathbf{p}') + \hat{V}_M(\mathbf{p}, \mathbf{p}'). \quad (29)$$

The first term on the right-hand side is the kinetic energy operator, and the second one is the interacting nonlocal potential defined according to

$$\begin{aligned} \hat{V}_M(\mathbf{p}, \mathbf{p}') &= -\gamma' \phi(\mathbf{p}) \phi(\mathbf{p}') e^{-i\mathbf{R}_2 \cdot (\mathbf{p} - \mathbf{p}')} \\ & \quad - \gamma' \phi(\mathbf{p}) \phi(\mathbf{p}') e^{-i\mathbf{R}_1 \cdot (\mathbf{p} - \mathbf{p}')}. \end{aligned} \quad (30)$$

This potential describes the interaction between the active electron and each of the nuclei of the molecule, and depends on the internuclear relative vector position  $\mathbf{R} = \mathbf{R}_2 - \mathbf{R}_1$ . The function  $\phi(\mathbf{p}) = \frac{1}{\sqrt{p^2 + \Gamma^2}}$  is the same auxiliary function used in [49,50]. The parameters  $\gamma' = \frac{\gamma}{2}$  and  $\Gamma$  are constants related with the shape of the ground state (for more details, see [50]).

By using  $\hat{H}(\mathbf{p}, \mathbf{p}')$  from Eq. (29), we write the stationary Schrödinger equation as follows:

$$\begin{aligned} \hat{H}_M(\mathbf{p}, \mathbf{p}') \Psi_{0M}(\mathbf{p}) &= \int d^3 \mathbf{p}' \hat{H}_M(\mathbf{p}, \mathbf{p}') \Psi_{0M}(\mathbf{p}'), \\ \left( \frac{p^2}{2} + I_p \right) \Psi_{0M}(\mathbf{p}) &= \gamma' \phi(\mathbf{p}) e^{-i\mathbf{R}_2 \cdot \mathbf{p}} \check{\phi}_1 + \gamma' \phi(\mathbf{p}) e^{-i\mathbf{R}_1 \cdot \mathbf{p}} \check{\phi}_2, \end{aligned} \quad (31)$$

where  $I_p$  denotes the ionization potential energy of the wave function  $\Psi_{0M}(\mathbf{p})$  which is related to the ground potential energy by  $E_0 = -I_p$ . To analytically solve Eq. (31), in the momentum representation, we consider

$$\check{\phi}_1 = \int d^3 \mathbf{p}' \Psi_{0M}(\mathbf{p}') \phi(\mathbf{p}') e^{i\mathbf{R}_2 \cdot \mathbf{p}'} = \int \frac{d^3 \mathbf{p}' \Psi_{0M}(\mathbf{p}') e^{i\mathbf{R}_2 \cdot \mathbf{p}'}}{\sqrt{p'^2 + \Gamma^2}}, \quad (32)$$

$$\check{\phi}_2 = \int d^3 \mathbf{p}' \Psi_{0M}(\mathbf{p}') \phi(\mathbf{p}') e^{i\mathbf{R}_1 \cdot \mathbf{p}'} = \int \frac{d^3 \mathbf{p}' \Psi_{0M}(\mathbf{p}') e^{i\mathbf{R}_1 \cdot \mathbf{p}'}}{\sqrt{p'^2 + \Gamma^2}}, \quad (33)$$

where the wave function for the bound states in momentum space  $\Psi_{0M}(\mathbf{p})$  is defined by

$$\Psi_{0M}(\mathbf{p}) = \frac{\gamma' \check{\phi}_1 e^{-i\mathbf{R}_2 \cdot \mathbf{p}}}{\sqrt{(p^2 + \Gamma^2)(\frac{p^2}{2} + I_p)}} + \frac{\gamma' \check{\phi}_2 e^{-i\mathbf{R}_1 \cdot \mathbf{p}}}{\sqrt{(p^2 + \Gamma^2)(\frac{p^2}{2} + I_p)}}. \quad (34)$$

Solving the system of Eqs. (32) and (33), we find that  $\check{\phi}_1 = \pm \check{\phi}_2$ . This relation let us two possible solutions, namely, symmetric and antisymmetric wave functions for  $\Psi_{0M}(\mathbf{p})$ .

Throughout this paper, we shall only consider the symmetric wave function as follows:

$$\Psi_{0M}(\mathbf{p}) = \frac{\mathcal{M}}{\sqrt{(p^2 + \Gamma^2)(\frac{p^2}{2} + I_p)}} \left[ 2 \cos\left(\frac{\mathbf{R} \cdot \mathbf{p}}{2}\right) \right], \quad (35)$$

where  $\mathcal{M} = \gamma' \check{\varphi}_1 = \frac{\gamma}{2} \check{\varphi}_1$  is a normalization constant. This constant is obtained by employing the conventional normalization condition for the bound states. Consequently, this factor thereby reads as

$$\mathcal{M} = \frac{1}{2} \left[ \frac{2\pi^2}{(2I_p - \Gamma^2)^2} \left\{ \frac{2e^{-R\Gamma}}{R} - \frac{2e^{-R\sqrt{2I_p}}}{R} - \frac{(2I_p - \Gamma^2)e^{-R\sqrt{2I_p}}}{\sqrt{2I_p}} + \frac{(\sqrt{2I_p} - \Gamma)^2}{\sqrt{2I_p}} \right\} \right]^{-1/2}. \quad (36)$$

With the exact dependency of  $\mathcal{M}$  we have well defined the bound state for our two-center molecular system. The wave function for the bound state can then be written as a combination of two *left* and *right* functions,  $\Psi_{0M}(\mathbf{p}) = \Psi_{0,L}(\mathbf{p}) + \Psi_{0,R}(\mathbf{p})$ , in agreement with the photoelectron transition amplitude derivation.  $\Psi_{0M}(\mathbf{p})$  then reads as:

$$\Psi_{0M}(\mathbf{p}) = \frac{\mathcal{M} e^{-i\mathbf{R}_1 \cdot \mathbf{p}}}{\sqrt{(p^2 + \Gamma^2)(\frac{p^2}{2} + I_p)}} + \frac{\mathcal{M} e^{-i\mathbf{R}_2 \cdot \mathbf{p}}}{\sqrt{(p^2 + \Gamma^2)(\frac{p^2}{2} + I_p)}}. \quad (37)$$

In the above wave function we can clearly see that each term contains information about only one of the nuclei. The first term corresponds to the electron-wave-function portion located at the atom on the *left* at  $\mathbf{R}_1 = -\frac{\mathbf{R}}{2}$ , meanwhile the second one to the electron portion placed on the *right* atom of the molecule at  $\mathbf{R}_2 = +\frac{\mathbf{R}}{2}$ , respectively. Equations (32) and (33) give us a relation between the electronic energy  $E_e$  of the molecular system and the internuclear distance  $R$  as follows:

$$\frac{2\pi^2\gamma}{R(\Gamma^2 - 2E_e)} [e^{-\sqrt{2E_e}R} - e^{-\Gamma R} + R(\Gamma - \sqrt{2E_e})] = 1. \quad (38)$$

In order to test the validity of the latter formulas, in Fig. 1 we show the potential energy surface (PES) of the diatomic molecule  $\text{H}_2^+$  as a function of internuclear distance. We depict the different energy contributions, electronic and nuclear, of the molecular system  $\text{H}_2^+$  obtained using the SFA model (left

panel) and the exact solution of the TDSE (right panel). While the electron-nuclei interaction is described by a kind of non-local short potential for our test molecular model, we choose as a repulsive potential between the nuclei a Yukawa one.

We stress that Fig. 1 is in very good agreement with the PES reported in the literature [58]: it shows the minimum of equilibrium for an interatomic distance at  $R_0 = 2$  a.u. This value is a clear signal of the good description offered by our SFA model. When  $R$  is large, the two atoms are weakly interacting and the energy of the system is equal to the energy of the atomic hydrogen,  $-0.5$  a.u. As  $R$  becomes smaller, the interaction results stronger and the energy is large and negative. In this case, we say that a bond is formed between the atoms. At even smaller values of  $R$ , the internuclear repulsion is very large (red line), therefore, the energy is large and positive. It is a standard approach to use zero-range potentials as a caricature of the true Coulomb ones in SFA. In fact, this choice is perfectly legitimate within the SFA framework, where the atomic or molecular potential is neglected when the electron is moving in the continuum, but if we consequently take, for instance, delta potentials between the two protons in the  $\text{H}_2^+$  molecule, we would not have the possibility of stabilizing it for  $R \neq 0$ . For this reason, we employ a Yukawa potential, that is also a short-range caricature of the Coulomb potential, but it has a finite-range repulsive core, which combined with attractive electronic energy allows to reach the stabilization of our molecule for finite values of  $R$  in the Born-Oppenheimer approximation. By comparing our results with the TDSE, we could argue that our approximation appears to work perfectly well (see Sec. IV A for more details).

## B. Bound-continuum transition matrix element

So far we have analytically obtained the ground state of our two-center molecular system. It allows us to compute the bound-free transition dipole matrix element  $\mathbf{d}_L(\mathbf{p}_0)$  and  $\mathbf{d}_R(\mathbf{p}_0)$  by using Eq. (9). By approximating the free or continuum state as a plane wave with a given momentum  $\mathbf{p}_0$ , the bound-free transition dipole matrix in the momentum representation reads as

$$\begin{aligned} \mathbf{d}_L(\mathbf{p}_0) &= -i\nabla_{\mathbf{p}} \Psi_{0,L}(\mathbf{p})|_{\mathbf{p}_0} + \mathbf{R}_1 \Psi_{0,L}(\mathbf{p}_0) \\ &= -2i \mathcal{M} \mathcal{A}(\mathbf{p}_0) e^{-i\mathbf{R}_1 \cdot \mathbf{p}_0}, \end{aligned} \quad (39)$$

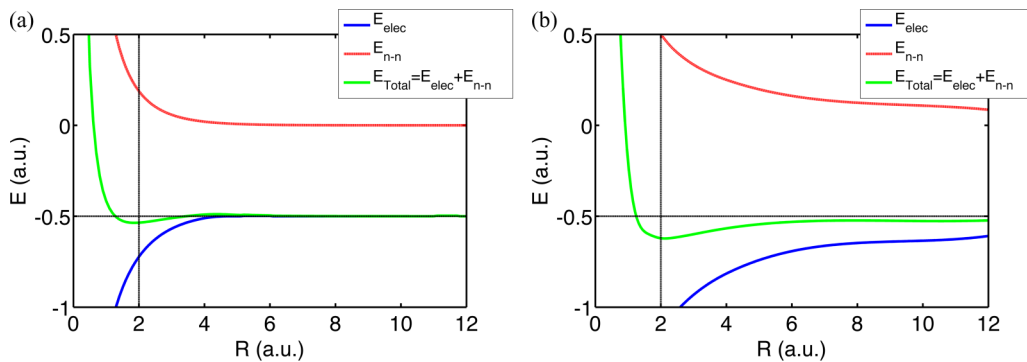


FIG. 1. Potential energy surface (PES) for the diatomic molecule  $\text{H}_2^+$  as a function of the internuclear distance. (a) Electronic energy (blue line) calculated using Eq. (38), nuclear-nuclear energy (red line), and total energy of the system (green line) obtained with the SFA model. (b) The same as in (a) but computed by the numerical solution of the TDSE. The vertical dashed lines show the energy minimum corresponding to the equilibrium distance of the system (see the text for details).

for the atom on the *left*, meanwhile that for the one on the *right* it results  $\mathbf{d}_{\mathcal{R}}(\mathbf{v}) = -2i \mathcal{M} \mathcal{A}(\mathbf{p}_0) e^{-i\mathbf{R}_2 \cdot \mathbf{p}_0}$ . In both cases,  $\mathcal{A}(\mathbf{p}_0)$  is defined as

$$\mathcal{A}(\mathbf{p}_0) = \frac{-\mathbf{p}_0(3p_0^2 + 2I_p + 2\Gamma^2)}{(p_0^2 + \Gamma^2)^{\frac{3}{2}}(p_0^2 + 2I_p)^2}. \quad (40)$$

The second important quantity to be calculated before evaluating the whole transition amplitude  $b(\mathbf{p}, t)$  is the transition continuum-continuum matrix element  $\mathbf{g}_m(\mathbf{p}, \mathbf{p}')$ . Hence, we need to find the scattering or continuum wave functions of our model potential. Next, we shall calculate them by analytically solving the time-independent Schrödinger equation in the momentum representation for positive energies.

### C. Scattering waves and the continuum-continuum transition matrix element

Let us consider a scattering wave  $\Psi_{\mathbf{M}\mathbf{p}_0}(\mathbf{p})$ , with asymptotic momentum  $\mathbf{p}_0$ , as a coherent superposition of a plane wave and an extra correction  $\delta\Psi_{\mathbf{M}\mathbf{p}_0}(\mathbf{p})$ :

$$\Psi_{\mathbf{M}\mathbf{p}_0}(\mathbf{p}) = \delta(\mathbf{p} - \mathbf{p}_0) + \delta\Psi_{\mathbf{M}\mathbf{p}_0}(\mathbf{p}). \quad (41)$$

This state has an energy  $E = \mathbf{p}_0^2/2$ . Then, the Schrödinger equation in momentum representation reads as

$$\left(\frac{p^2}{2} - \frac{p_0^2}{2}\right)\delta\Psi_{\mathbf{M}\mathbf{p}_0}(\mathbf{p}) = -\hat{V}_{\mathbf{M}}(\mathbf{p}, \mathbf{p}_0) - \int d^3\mathbf{p}' \hat{V}_{\mathbf{M}}(\mathbf{p}, \mathbf{p}')\delta\Psi_{\mathbf{M}\mathbf{p}_0}(\mathbf{p}'). \quad (42)$$

Inserting the nonlocal potential, Eq. (30), in Eq. (42) and after some algebra, we obtain

$$\begin{aligned} (p^2 - p_0^2)\delta\Psi_{\mathbf{M}\mathbf{p}_0}(\mathbf{p}) &= 2\gamma' \phi(\mathbf{p})\phi(\mathbf{p}_0)[e^{-i\mathbf{R}_2 \cdot (\mathbf{p} - \mathbf{p}_0)} + e^{-i\mathbf{R}_1 \cdot (\mathbf{p} - \mathbf{p}_0)}] \\ &+ 2\gamma'\check{\phi}'_1 \phi(\mathbf{p})e^{-i\mathbf{R}_2 \cdot \mathbf{p}} + 2\gamma'\check{\phi}'_2 \phi(\mathbf{p})e^{-i\mathbf{R}_1 \cdot \mathbf{p}}, \end{aligned} \quad (43)$$

where the variables  $\check{\phi}'_1$  and  $\check{\phi}'_2$  are defined by

$$\check{\phi}'_1 = \int d^3\mathbf{p}' \delta\Psi_{\mathbf{M}\mathbf{p}_0}(\mathbf{p}')\phi(\mathbf{p}')e^{i\mathbf{R}_2 \cdot \mathbf{p}'} = \int \frac{d^3\mathbf{p}' \delta\Psi_{\mathbf{M}\mathbf{p}_0}(\mathbf{p}')e^{i\mathbf{R}_2 \cdot \mathbf{p}'}}{\sqrt{p'^2 + \Gamma^2}}, \quad (44)$$

$$\check{\phi}'_2 = \int d^3\mathbf{p}' \delta\Psi_{\mathbf{M}\mathbf{p}_0}(\mathbf{p}')\phi(\mathbf{p}')e^{i\mathbf{R}_1 \cdot \mathbf{p}'} = \int \frac{d^3\mathbf{p}' \delta\Psi_{\mathbf{M}\mathbf{p}_0}(\mathbf{p}')e^{i\mathbf{R}_1 \cdot \mathbf{p}'}}{\sqrt{p'^2 + \Gamma^2}}. \quad (45)$$

Finally, for  $\delta\Psi_{\mathbf{M}\mathbf{p}_0}$  we write

$$\begin{aligned} \delta\Psi_{\mathbf{M}\mathbf{p}_0}(\mathbf{p}) &= \frac{D_1(\mathbf{p}_0) e^{-i\mathbf{R}_2 \cdot (\mathbf{p} - \mathbf{p}_0)} - D_2(\mathbf{p}_0) e^{-i\mathbf{R}_2 \cdot (\mathbf{p} + \mathbf{p}_0)}}{\sqrt{p^2 + \Gamma^2}(p_0^2 - p^2 + i\epsilon)} \\ &+ \frac{D_1(\mathbf{p}_0) e^{-i\mathbf{R}_1 \cdot (\mathbf{p} - \mathbf{p}_0)} - D_2(\mathbf{p}_0) e^{-i\mathbf{R}_1 \cdot (\mathbf{p} + \mathbf{p}_0)}}{\sqrt{p^2 + \Gamma^2}(p_0^2 - p^2 + i\epsilon)}, \end{aligned} \quad (46)$$

where  $\epsilon$  is another infinitesimal parameter to avoid the divergence at the “energy shell”  $p^2 = p_0^2$ . The singularity at the “energy shell” is avoided due to the finite spread of

the involved wave packets. In numerical calculations we set throughout this paper  $\epsilon = 0.4$  a.u. (for more details, see [50]). The integration “constants” for the scattering states in Eq. (46) have the following dependency:

$$\begin{aligned} D_1(\mathbf{p}_0) &= \frac{\gamma}{\sqrt{p_0^2 + \Gamma^2}} \left\{ \frac{1 + I_1}{I_2^2 - (1 + I_1)^2} \right\}; \\ D_2(\mathbf{p}_0) &= \frac{\gamma}{\sqrt{p_0^2 + \Gamma^2}} \left\{ \frac{I_2}{I_2^2 - (1 + I_1)^2} \right\}, \end{aligned} \quad (47)$$

where

$$I_1 = \frac{-2\pi^2 \gamma}{\Gamma - i\sqrt{|p_0^2 + i\epsilon|}}, \quad (48)$$

$$I_2 = \frac{-2\pi^2 \gamma}{R(p_0^2 + \Gamma^2 + i\epsilon)} [e^{iR\sqrt{p_0^2 + i\epsilon}} - e^{-R\Gamma}]. \quad (49)$$

Finally, the molecular scattering wave function can be written as a composition of two contributions, namely,

$$\Psi_{\mathbf{M}\mathbf{p}_0}(\mathbf{p}) = \delta(\mathbf{p} - \mathbf{p}_0) + \delta\Psi_{\mathcal{R}\mathbf{p}_0}(\mathbf{p}) + \delta\Psi_{\mathcal{L}\mathbf{p}_0}(\mathbf{p}), \quad (50)$$

where

$$\delta\Psi_{\mathcal{L}\mathbf{p}_0}(\mathbf{p}) = \frac{D_1(\mathbf{p}_0) e^{-i\mathbf{R}_1 \cdot (\mathbf{p} - \mathbf{p}_0)} - D_2(\mathbf{p}_0) e^{-i\mathbf{R}_1 \cdot (\mathbf{p} + \mathbf{p}_0)}}{\sqrt{p^2 + \Gamma^2}(p_0^2 - p^2 + i\epsilon)}, \quad (51)$$

$$\delta\Psi_{\mathcal{R}\mathbf{p}_0}(\mathbf{p}) = \frac{D_1(\mathbf{p}_0) e^{-i\mathbf{R}_2 \cdot (\mathbf{p} - \mathbf{p}_0)} - D_2(\mathbf{p}_0) e^{-i\mathbf{R}_2 \cdot (\mathbf{p} + \mathbf{p}_0)}}{\sqrt{p^2 + \Gamma^2}(p_0^2 - p^2 + i\epsilon)}. \quad (52)$$

Equation (51) describes electrons that have probability of scatter with the ion core placed at  $\mathbf{R}_1$ . Similarly, Eq. (52) represents a scattering process with the nucleus placed at  $\mathbf{R}_2$ .

Let us consider the scattering waves obtained in Eqs. (51) and (52) to evaluate the continuum-continuum transition matrix element of Eq. (12). After some algebra it reads as

$$\begin{aligned} \mathbf{g}_m(\mathbf{p}_1, \mathbf{p}_2) &= \mathcal{Q}_1(\mathbf{p}_1, \mathbf{p}_2)[e^{-i\mathbf{R}_1 \cdot (\mathbf{p}_1 - \mathbf{p}_2)} + e^{-i\mathbf{R}_1 \cdot (\mathbf{p}_1 - \mathbf{p}_2)}] \\ &+ \mathcal{Q}_2(\mathbf{p}_1, \mathbf{p}_2)[e^{-i\mathbf{R}_1 \cdot (\mathbf{p}_1 + \mathbf{p}_2)} + e^{-i\mathbf{R}_2 \cdot (\mathbf{p}_1 + \mathbf{p}_2)}], \end{aligned} \quad (53)$$

where

$$\mathcal{Q}_1(\mathbf{p}_1, \mathbf{p}_2) = i[D_1(\mathbf{p}_2)\mathcal{C}_1(\mathbf{p}_1, \mathbf{p}_2) - D_1^*(\mathbf{p}_1)\mathcal{C}_2(\mathbf{p}_1, \mathbf{p}_2)], \quad (54)$$

$$\mathcal{Q}_2(\mathbf{p}_1, \mathbf{p}_2) = -i[D_2(\mathbf{p}_2)\mathcal{C}_1(\mathbf{p}_1, \mathbf{p}_2) - D_2^*(\mathbf{p}_1)\mathcal{C}_2(\mathbf{p}_1, \mathbf{p}_2)], \quad (55)$$

and

$$\begin{aligned} \mathcal{C}_1(\mathbf{p}_1, \mathbf{p}_2) &= \left[ \frac{\mathbf{p}_1(3p_1^2 - p_2^2 + 2\Gamma^2)}{(p_1^2 + \Gamma^2)^{\frac{3}{2}}(p_2^2 - p_1^2 + i\epsilon)^2} \right], \\ \mathcal{C}_2(\mathbf{p}_1, \mathbf{p}_2) &= \left[ \frac{\mathbf{p}_2(3p_2^2 - p_1^2 + 2\Gamma^2)}{(p_2^2 + \Gamma^2)^{\frac{3}{2}}(p_1^2 - p_2^2 - i\epsilon)^2} \right]. \end{aligned} \quad (56)$$

Equation (53) can be recast as:

$$\mathbf{g}_{\mathcal{L}}(\mathbf{p}_1, \mathbf{p}_2) = \mathbf{g}_{\mathcal{L}\mathcal{L}}(\mathbf{p}_1, \mathbf{p}_2) + \mathbf{g}_{\mathcal{L}\mathcal{R}}(\mathbf{p}_1, \mathbf{p}_2)$$

and

$$\mathbf{g}_{\mathcal{R}}(\mathbf{p}_1, \mathbf{p}_2) = \mathbf{g}_{\mathcal{R}\mathcal{R}}(\mathbf{p}_1, \mathbf{p}_2) + \mathbf{g}_{\mathcal{R}\mathcal{L}}(\mathbf{p}_1, \mathbf{p}_2)$$

where

$$\begin{aligned}\mathbf{g}_{\mathcal{L}\mathcal{L}}(\mathbf{p}_1, \mathbf{p}_2) &= \mathcal{Q}_1(\mathbf{p}_1, \mathbf{p}_2) e^{-i\mathbf{R}_1 \cdot (\mathbf{p}_1 - \mathbf{p}_2)}, \\ \mathbf{g}_{\mathcal{L}\mathcal{R}}(\mathbf{p}_1, \mathbf{p}_2) &= \mathcal{Q}_2(\mathbf{p}_1, \mathbf{p}_2) e^{i\mathbf{R}_1 \cdot (\mathbf{p}_1 + \mathbf{p}_2)}, \\ \mathbf{g}_{\mathcal{R}\mathcal{R}}(\mathbf{p}_1, \mathbf{p}_2) &= \mathcal{Q}_1(\mathbf{p}_1, \mathbf{p}_2) e^{-i\mathbf{R}_2 \cdot (\mathbf{p}_1 + \mathbf{p}_2)},\end{aligned}$$

and

$$\mathbf{g}_{\mathcal{R}\mathcal{L}}(\mathbf{p}_1, \mathbf{p}_2) = \mathcal{Q}_2(\mathbf{p}_1, \mathbf{p}_2) e^{i\mathbf{R}_2 \cdot (\mathbf{p}_1 - \mathbf{p}_2)}.$$

From these last equations we can identify all the contributions, i.e., local,  $\mathbf{g}_{\mathcal{L}\mathcal{L}/\mathcal{R}\mathcal{R}}(\mathbf{p}_1, \mathbf{p}_2)$ , and nonlocal and cross,  $\mathbf{g}_{\mathcal{L}\mathcal{R}/\mathcal{R}\mathcal{L}}(\mathbf{p}_1, \mathbf{p}_2)$ , respectively. After obtaining both the bound-free and continuum-continuum transition matrix elements, it is possible to compute Eqs. (15) and (20) to obtain the direct, the rescattering, and the total photoelectron transition amplitudes. The presented model is an alternative way to describe the ATI process mediated by a strong laser pulse. Our two-center molecular model is an extension to the one presented in Ref. [50] and renders to the same atomic equations when  $\mathbf{R}$  is close to zero (see Appendix for more details and proofs).

We stress that the method is physically intuitive, and can be understood on the basis of a quasiclassical picture, i.e., electron trajectories. This is the main difference of our approach in comparison to the numerical solution of the TDSE, whose physical interpretation is, in spite of its accuracy, frequently challenging. The main advantage of the proposed model is that Eqs. (15) and (20) give a clear physical understanding of the ATI process and provide rich and useful information about both the laser field and the diatomic molecular target, which are encoded into the complex transition amplitude  $b(\mathbf{p}, t) = b_0(\mathbf{p}, t) + b_1(\mathbf{p}, t)$ . The exact analytical solutions of both the direct and rescattering transition amplitudes are, however, not trivial to obtain if no approximations are considered. In particular, for the rescattering photoelectrons, the solution is even more complex and depends, generally, of the laser electric field shape.

#### IV. RESULTS AND DISCUSSION

Along this section we shall compare the outcomes of our model for the ATI spectra emitted from a  $\text{H}_2^+$  system to the exact numerical solution of the 3D-TDSE. A scan on different internuclear distances of the ionization probability and the whole momentum distribution along the polarization laser and molecular orientation axis shows that our model works reasonably well. Furthermore, split of contributions coming from the left and right nuclei and local, cross, and nonlocal rescattering processes help to distinguish which part of the photoelectron spectra is relevant for each kind of event. The molecular internuclear distance is retrieved probing that our model is capable to capture the structural information encoded on the photoelectron spectra.

Finally, experimental photoelectron spectra on the  $\text{O}_2^+$  molecule driven by a mid-IR source (3.1  $\mu\text{m}$ ) demonstrate that our simplified model is able to render the main physics behind the rescattering process in a more “complex” symmetric diatomic molecule.

#### A. Comparison of SFA and TDSE models

The numerical integration for the photoelectron spectra computation by means of Eqs. (15) and (20) has been performed via a rectangular rule with particular emphasis on the convergence of the results. As the final momentum distribution, Eq. (25), is “locally” independent of the momentum  $\mathbf{p}$ ,  $|b(\mathbf{p}, t)|^2$  can be computed concurrently for a given set of  $\mathbf{p}$  values. We have optimized the calculation of the whole transition amplitude  $|b(\mathbf{p}, t)|^2$  by using the OPENMP parallel package [59] and the MPI paradigm [60]. The final momentum photoelectron distribution  $|b(\mathbf{p}, t)|^2$  is computed both in a 1D momentum line along  $p_z$ , and in a 2D momentum plane ( $p_y, p_z$ ). We shall compare these results with the numerical solution of the TDSE. We fix the parameters of the nonlocal potential to  $\Gamma = 1.0$  and  $\gamma = 0.1$  a.u. Such values describe the potential energy surface of Fig. 1, which is in good agreement with the expected energy dependency of the  $\text{H}_2^+$  molecular system. We use in our simulations an ultrashort laser pulse with central frequency  $\omega_0 = 0.057$  a.u. (wavelength  $\lambda = 800$  nm, photon energy 1.55 eV), with a  $\sin^2$  envelope shape with  $N_c = 4$  total cycles (this corresponds to a full-width at half-maximum FWHM = 5.2 fs) and a CEP  $\phi_0 = 0$  rad. The time step is fixed to  $\delta t = 0.02$  a.u., and the numerical integration time window is  $t \in [0, t_F]$ , where  $t_F = N_c T_0 \approx 11$  fs and  $T_0 = 2\pi/\omega_0$  denote the final “detection” time and the cycle period of the laser field, respectively.

In addition, we perform the numerical integration of the 3D-TDSE by using the Crank-Nicolson algorithm in cylindrical coordinates  $(\rho, z)$  where the polar angle  $\varphi$  is neglected. This is well justified by considering the laser field is linearly polarized along the molecular  $z$  axis and the fact that the magnetic momentum electron-quantum number  $m$  remains as a conserved quantity during the whole evolution of the system. Thereby, the electronic Hamiltonian of our system is  $\hat{H} = \frac{\hat{p}_\rho^2}{2} + \frac{\hat{p}_z^2}{2} + \hat{V}(\rho, z) + zE(t)$ . For the present numerical solution of the TDSE, we have fixed the position grid step to  $\delta\rho = \delta z = 0.2$  a.u., with a total number of points for the  $\rho$  axis of  $N_\rho = 6000$  and the  $z$  axis of  $N_z = 12000$ , respectively. The ground state is computed via imaginary-time propagation with a time step of  $\delta t = -0.02 i$  and the Coulomb potential for our two-center molecule is given by  $V(\rho, z) = -\frac{1}{\sqrt{\rho^2 + (z+R/2)^2}} - \frac{1}{\sqrt{\rho^2 + (z-R/2)^2}}$ . The strong-field laser-molecule interaction is simulated by evolving the electronic ground-state wave function in real time, with a time step of  $\delta t = 0.02$  a.u., and under the action of both the molecular potential and the laser electric field. At the end of the laser pulse  $t_F$ , when the laser electric field is zero, we compute the final photoelectron energy-momentum distribution  $|b_{\text{TDSE}}(p_\rho, p_z, t_F)|^2$  by projecting the “free”-electron wave packet  $\Psi_c(\rho, z, t_F)$  over plane waves. The wave packet  $\Psi_c(\rho, z, t_F)$  is calculated by smoothly masking the bound states from the entire wave function  $\Psi(\rho, z, t_F)$ .

First, and in order to test if our model is capable to capture the final photoelectron spectrum of the ATI processes, we compare our SFA model to the numerical solution of the 3D-TDSE for the simplified case of  $\text{H}_2^+$ . Figure 2 depicts such comparison. In Fig. 2(a), we calculate a scan of the ionization probability over a set of 15 interatomic

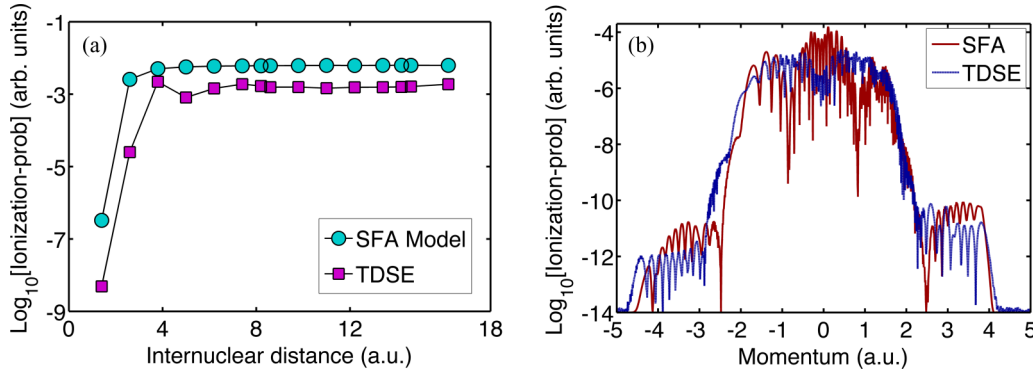


FIG. 2. (a) Ionization probability (in logarithmic scale) as a function of the internuclear distance  $R$  calculated using the SFA (circle magenta) and the TDSE (square light blue) for  $I_0 = 4 \times 10^{14} \text{ W cm}^{-2}$ . (b) Full transition amplitude  $|b(p_z, t_F)|^2$  as a function of the photoelectron final momentum, calculated using the SFA model (red line) and ATI computed by the numerical solution of the TDSE (blue line) (see the text for details).

distances. Note that by ionization probability the reader should understand the final-time integral momentum distribution of the whole transition probability amplitude, Eq. (25). Here, we set the molecular axis parallel to the laser electric field polarization. Those results show a reasonable agreement between the SFA and TDSE models, particularly for larger internuclear distances, when the details of the potential are not important. In both calculations we can observe that for shorter distances the ionization probability is strongly dependent on the relative position of the atoms inside the molecule. The ionization probability scales almost exponentially (note that the scale is logarithmic) and increases rapidly, when the atoms are close to each other, at  $R \lesssim 4$  a.u. Both models present the same trend, namely, a low-ionization probability for shorter distances, followed by a rapid increasing, and a sort of “stabilization” for larger internuclear distances. The physical picture of this behavior is as follows: the electron is tightly (loosely) bounded for small (larger) internuclear distances. According to the Keldysh-Faisal-Reiss model, the electrons have less probability to be ionized by tunneling effect [51–53] for potentials with larger  $I_p$ , which of course in this molecular case corresponds to small internuclear distances. Note that we mean small or large internuclear distances  $R$  in comparison to the equilibrium one  $R_0$  ( $R_0 = 2.0$  a.u. for our  $\text{H}_2^+$  molecule). Furthermore, the same tendency of both the SFA and the 3D-TDSE in the whole internuclear distances range is observed, except a constant factor, which clearly indicates the difference between the short-range (SFA) and long-range (TDSE) potentials. Further, the ionization probability shows a stabilization value (around  $10^{-3}$  arb. units for both cases) from which it remains constant regardless the value of  $R$ .

The previous comparison only describes the final photoelectron spectra dependence on the internuclear distance. A better scenario to evaluate the quality of our model, however, can be employed, namely, a one-to-one analysis of the ATI momentum distributions. The aim is to confirm if our model is able to capture both the interference nature of the ATI spectra for molecules and the underlying electron dynamics. In Fig. 2(b), we show results of the photoelectron momentum spectra computed by our quasiclassical model and the TDSE along the momentum line  $\mathbf{p} = (0, 0, p_z)$  at  $R = 3.8$  a.u. As in Fig. 2(a), we observe an excellent agreement between both

models. It means that our quasiclassical approach is able to provide a reasonable good description of the whole ATI processes. We can argue that the two models are describing the same physics: stronger oscillations for small values of momentum followed by a rapid decrease of the ATI yield (at  $|p_z| \lesssim 2.5$  a.u.), a plateau, where the amplitude remains almost constant, and both approaches end up with an abrupt cutoff around the same value of  $|p_z| \lesssim 4$  a.u.

One of the main advantages of our SFA model is the possibility to disentangle the different contributions to the final ATI spectra (for details, see previous sections). In Fig. 3, we show the different contributions, in logarithmic scale, as a function of the ponderomotive energy  $U_p$  for electrons with negative momenta along the  $p_z$  direction and for a fixed value of  $R$ , close to the equilibrium distance  $R_0 = 2.0$  a.u. Figure 3(a) shows the main contributions to the full final photoelectron spectra: the total  $|b(\mathbf{p}, t)|^2$  [Eq. (25)], the direct  $|b_0(\mathbf{p}, t)|^2$  [Eq. (17)], and the rescattering  $|b_1(\mathbf{p}, t)|^2$  [Eq. (22)] terms, respectively. In the same way in Fig. 3(b) we plot the two terms  $|b_{0,\mathcal{L}}(\mathbf{p}, t)|^2$  and  $|b_{0,\mathcal{R}}(\mathbf{p}, t)|^2$  which contribute to the direct process. The terms that play an important role in the rescattering process  $|b_{\text{local}}(\mathbf{p}, t)|^2$  [Eq. (23)] and  $|b_{\text{nonlocal+cross}}(\mathbf{p}, t)|^2$  [Eq. (24)] are displayed in Fig. 3(c). As we can infer from the latter figure, the main contribution to the rescattering term is from the local processes (see Sec. II). Finally, in Fig. 3(d) we show the two processes contributing to the local one. For this calculation we have considered the molecule aligned in the same direction as the laser electric field polarization, i.e., the internuclear distance vector has only a  $z$  component  $\mathbf{R} = (0, 0, R_z)$ .

Our second clear observation in Fig. 3 is that each term contributes to different regions of the photoelectron spectra, i.e., for electron energies  $E_p \lesssim 4U_p$  the direct term  $|b_0(\mathbf{p}, t)|^2$  dominates the spectrum and, on the contrary, it is the rescattering term  $|b_1(\mathbf{p}, t)|^2$  the one that prevails in the high-energy electron region. The photoelectron spectra show the expected two cutoffs defined by  $2U_p$  and  $10U_p$  (black dashed lines) which are presented in the atomic and molecular ATI process [21,49]. As a consequence of this last observation we can safely argue that our approach is a reliable alternative for the calculation of photoelectron spectra in molecules. For the direct process, Fig. 3(b), we observe that

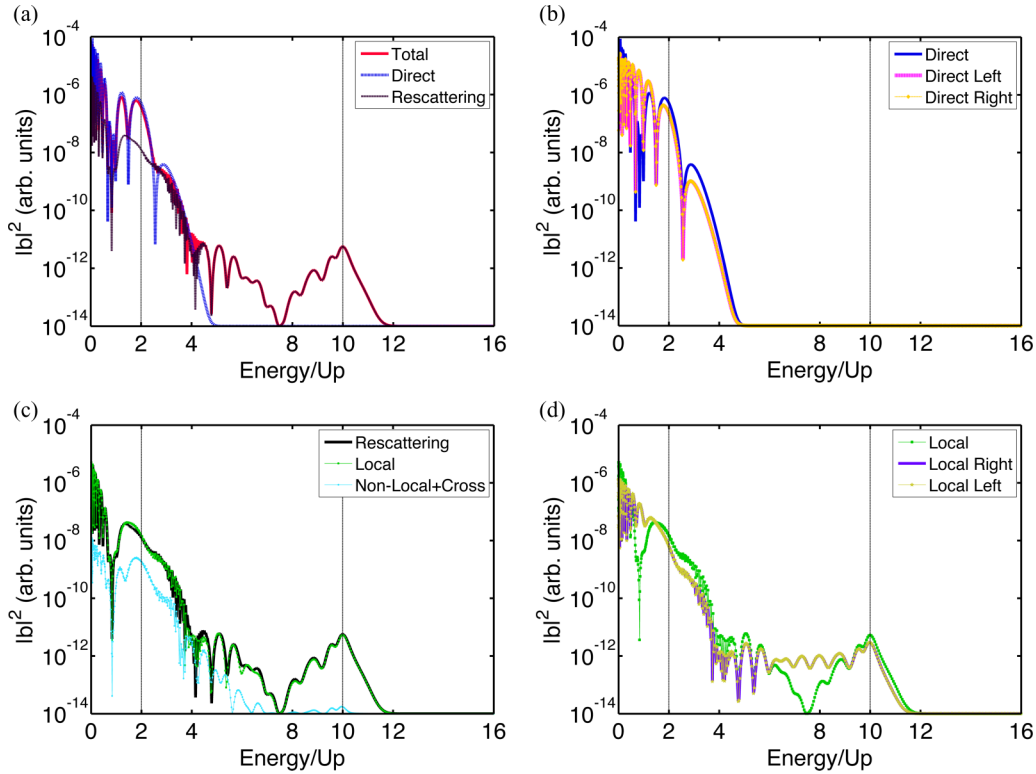


FIG. 3. Terms contributions to the photoelectron spectra (in logarithmic scale) as a function of the ratio between electron energy and ponderomotive energy  $U_p$  calculated by using our quasiclassical SFA model for  $R = 2.6$  a.u. The peak laser intensity used in this calculation is set to  $I_0 = 4 \times 10^{14}$  W cm $^{-2}$ . (a) Total, direct, and rescattering terms; (b) direct, direct left, and direct right terms; (c) rescattering, local, and nonlocal+cross terms; (d) local, local right, and local left terms (see the text for more details).

both the direct *left* and direct *right* terms contribute within a comparable energy range. In addition, both terms show the same behavior, having exactly the same energy for the interference minimum: the coherent sum of these two terms, the total direct contribution (solid blue line), has a deeper minimum value around 1.0 a.u. In Fig. 3(c), we observe that the local term (green dotted line) contributes mostly in the low-energy region of the ATI spectrum. Furthermore, the nonlocal and cross terms do not contribute for electron energies  $E_p \gtrsim 6U_p$ . It is also demonstrated that the contribution of  $|b_{\text{nonlocal+cross}}(\mathbf{p}, t)|^2$  becomes even less important for larger internuclear distances as it is expected. Finally, in Fig. 3(d) we show that the local right and local left contributions have the same shape and contribute to the whole energy range.

Having in mind a deeper analysis of the ATI processes, we extend our numerical calculations from a 1D momentum line (Fig. 3) to a 2D momentum plane. The results of our computations are shown in Fig. 4. Here, we depict the different contributions using our analytical quasiclassical ATI model. For this calculation we use a laser field with a peak intensity of  $I_0 = 1 \times 10^{14}$  W cm $^{-2}$  and the internuclear distance is set to  $R = 4.2$  a.u.

The 2D calculations resemble the features of the 1D ones: the low momenta region of the spectrum is dominated by the direct process [Fig. 4(a)], meanwhile the rescattering term, dominated by the local processes, is important for large electron momenta [Fig. 4(c)]. Furthermore, the nonlocal and cross [Fig. 4(b)] processes can be neglected when compared to the local processes. In all the figures we clearly distinguish the

position of a deep minimum about an electron momentum  $p = 0.74$  a.u. (the corresponding energy is  $E = p^2/2 = 1.23U_p$ ) and the well-known asymmetric rings. Furthermore, we observe a symmetry of the structures about the  $p_y$  axis for all the terms and a left-right asymmetric for electrons with  $p_z < 0$  or  $p_z > 0$ . As was already mentioned, one of the advantages of our diatomic SFA model is that it allows us to account for the individual contributions to the ATI spectrum. In addition, aside from being analytically formulated, our model is able to switch on and off each of the ionization mechanisms which build up the final total and experimentally accessible ATI momentum spectrum  $|b(p_z, p_y, t_F)|^2$ .

As was mentioned at the outset, one of the main concerns with our model is to find a way to retrieve structural information of the molecular system starting from the ATI spectra. In the following we perform a detailed analysis of the interference pattern for different internuclear distances. Here, the well-known two-slit interference formula  $p = \frac{(2n+1)\pi}{R \cos \theta}$  [40] is used in order to extract the internuclear distance from the interference pattern present in the photoelectron spectra.

In Fig. 5, we show the photoelectron distribution or ATI spectra  $[|b(p, t)|^2]$ , in logarithmic scale, as a function of the final electron momentum for different internuclear distances. Figure 5(a) depicts the ATI spectra for a large value of the internuclear distance:  $R = 14.2$  a.u., in order to see a considerable number of interference minima. Furthermore, the ATI spectra in Fig. 5(b) are computed varying the internuclear distance  $R$  (see the panel labels for the values). The dashed black lines represent the expected minima calculated by

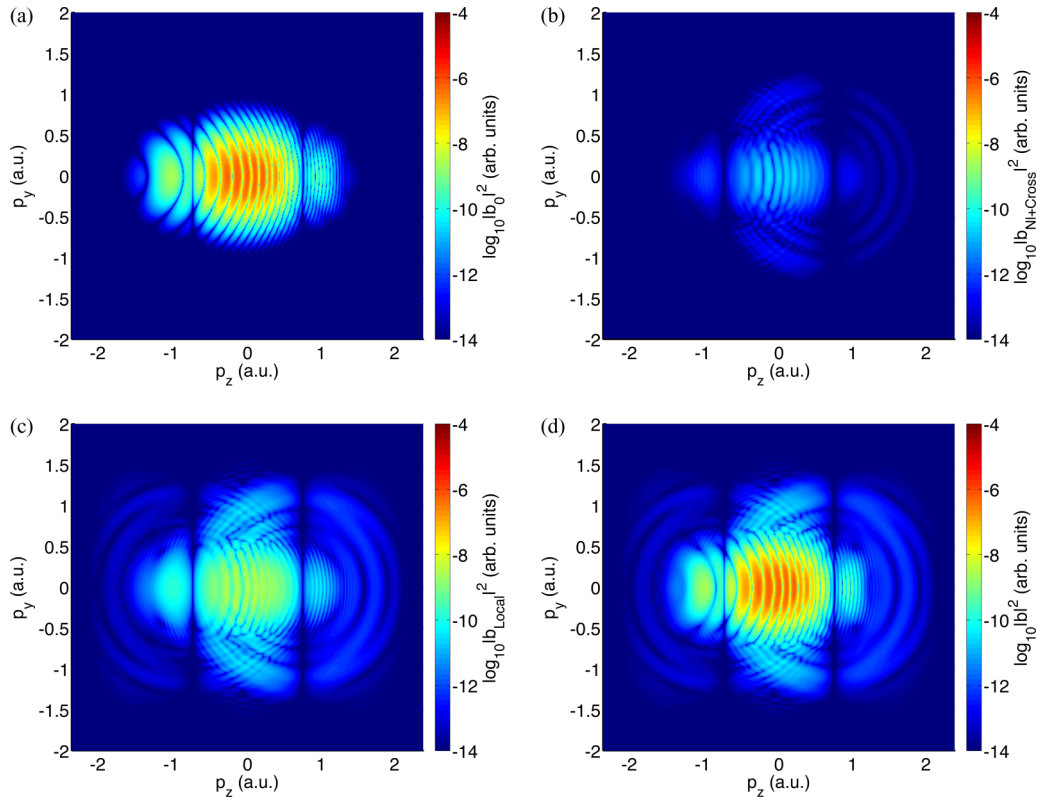


FIG. 4. Different contributions to the photoelectron spectra for a 2D momentum plane ( $p_z, p_y$ ). ATI photoelectron spectra (in logarithmic scale) as a function of the momentum ( $p_z, p_y$ ) computed by our quasiclassical model for each term. (a) Direct term, (b) nonlocal and cross terms, (c) local term, and (d) total contribution. We use a laser field with a peak intensity of  $I_0 = 1 \times 10^{14} \text{ W cm}^{-2}$  and the internuclear distance is set to  $R = 4.2 \text{ a.u.}$

applying the two-slit interference formula. As it is observed, our model is able to reproduce all the interference minima and this is a clear evidence that the photoelectron spectra contains structural information of the molecular system.

### B. Theory versus experimental results

In order to conclude our analysis and as an additional validation of our model, we compare the results computed

using the SFA approach with experimental data obtained at ICFO for  $\text{O}_2^+$  molecules [61]. The experimental data were taken for randomly oriented molecules and the laser pulse was CEP randomized, i.e., an average of the theoretical results over both the molecular orientations and different CEP values is required for an accurate theoretical description. The reported laser peak intensity and wavelength are  $I_0 = 8.5 \times 10^{13} \text{ W cm}^{-2}$  and  $\lambda = 3.1 \mu\text{m}$ , respectively. The laser pulse has a

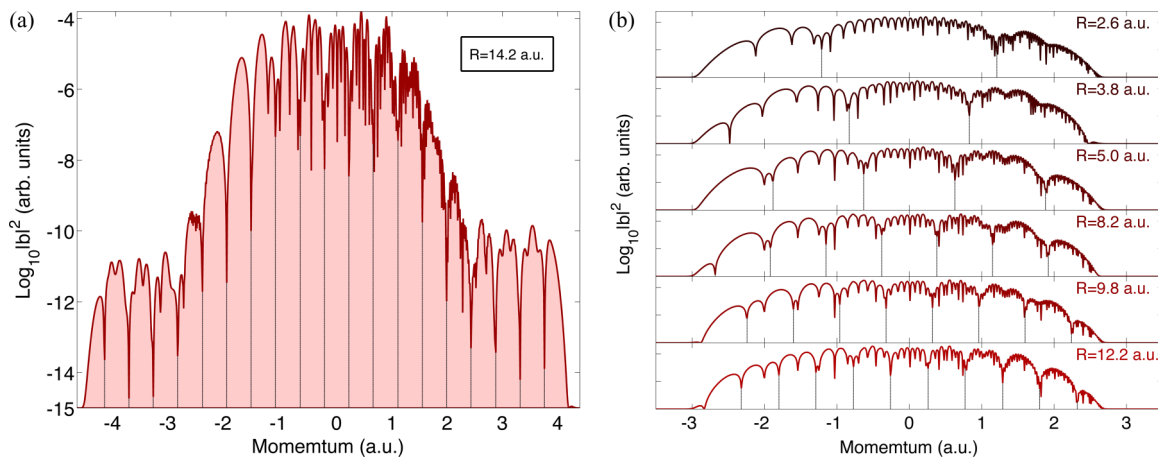


FIG. 5. ATI spectra calculated using the SFA model for an intensity value of  $I_0 = 4 \times 10^{14} \text{ W cm}^{-2}$ , as a function of the momentum. (a) Photoelectron spectra computed for  $R = 14.2 \text{ a.u.}$ ; (b) the same as (a) but for an internuclear range  $R = [2.6, 12.2] \text{ a.u.}$  The vertical lines in both panels indicate the position of the interference minima (see the text for details).

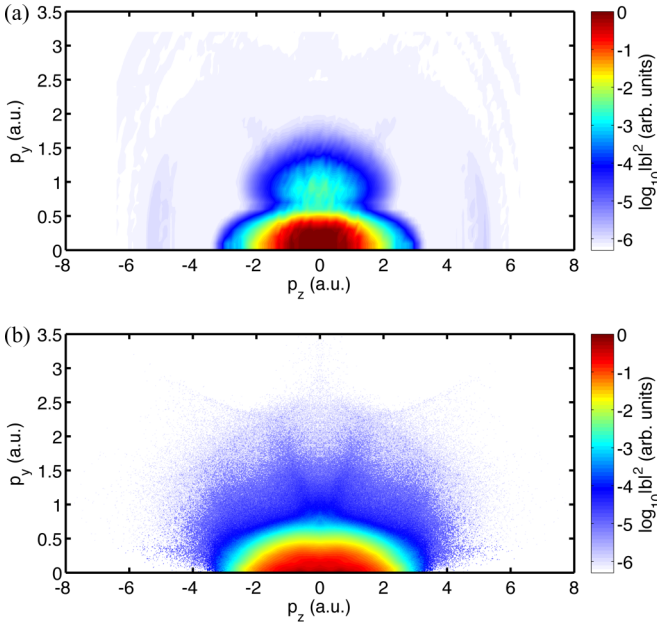


FIG. 6. Photoelectron spectra for the  $O_2^+$  molecule. (a) ATI spectra calculated using the SFA model; (b) experimental ATI spectra obtained in the attosecond and ultrafast optics group at ICFO [61]. In the theoretical calculations, the laser peak intensity, wavelength, and total time duration are  $I_0 = 8.5 \times 10^{13} \text{ W cm}^{-2}$ ,  $\lambda = 3.1 \mu\text{m}$ , and 52 fs (5 optical cycles), respectively. The dynamic range of the experimental data as shown here was adapted to the theoretical simulation for an adequate comparison. In addition, the internuclear distance is set to  $R = 2.21 \text{ a.u.}$  ( $1.17 \text{ \AA}$ ) (see the text for details).

duration of 75 fs full-width at half-maximum at a repetition rate of 160 kHz. Furthermore, the O–O bond length is retrieved from the photoelectron spectra and set to a value  $R = 1.17 \text{ \AA}$  ( $2.21 \text{ a.u.}$ ) [61]. This value of  $R$  corresponds to an ionization potential energy of  $I_p = 0.93 \text{ a.u.}$  and, in order to reproduce this value, in our model we set the parameters of the nonlocal potential  $\Gamma = 0.75$  and  $\gamma = 0.097 \text{ a.u.}$  With these values we obtain a very good fit to the dissociation energy  $E_d = 18.5 \text{ eV}$ , and the equilibrium internuclear distance  $R = 1.116 \text{ \AA}$  ( $2.11 \text{ a.u.}$ ), reported in the literature [62].

In order to accurately compare with the experimental measurements, the calculated ATI spectra are averaged over the orientation of the molecule with respect to the laser-polarization axis, using eight values of the orientation angle  $\theta$  in the range  $[0^\circ-360^\circ]$ . In addition, an average over the CEP values, and for the same orientation range, is considered. For symmetry considerations, only 16 different sets of photoelectron spectra are computed. For each set a total of 8192 points in the  $(p_z, p_y)$  plane are used. Around 150 000 CPU hours were employed for the whole ATI computation. For the comparison experiment versus theory, we employ the same laser peak intensity (no focal averaging is considered in the calculations) and the internuclear distance reported in the experiment for each calculation. The result of this comparison is depicted in Fig. 6.

In Fig. 6(a) we show the calculated total ionization probability  $|b(\mathbf{p}, t)|^2$  [Eq. (25)] and in Fig. 6(b) we present the experimental data. In order to make an easier comparison,

the theoretical calculations are multiplied by a constant factor. The plots show that our model is in very good agreement with the experimental measurements. In fact, both panels present the same color scales, covering six orders of magnitude. Both the simulated and measured data exhibit the same regions of signal, with comparable amplitudes for all the longitudinal momentum. In addition, a similar dome structure, around  $p_z = [-3; 3]$  and  $p_y = [0; 0.7]$ , is observed in both pictures. Note that the interference fringes are not observed either in the experimental or in the theoretical calculations. Thereby, the different recollision scenarios in terms of electron trajectories are washed out due to both the molecular orientation and CEP averages. We could trace out the theory versus experiment discrepancies considering that (i) our SFA model neglects Coulomb effects, which could be important in the low-energy region of the ATI spectrum; (ii) we are working within the SAE, i.e., our approach does not take into account any multielectron contributions, that could play a role in the photoelectron distributions, particularly for multielectronic molecules; (iii) we are not including a laser intensity focal average, i.e., in our calculations only one laser intensity is used in the simulations, contrarily with the experiment, where the atoms or molecules in the interaction region feel different laser intensities, due the intensity spatial distribution of the laser beam.

## V. CONCLUSIONS AND OUTLOOK

We have presented a simple and analytical model to describe the above-threshold ionization (ATI) process from a diatomic molecule while an ultraintense infrared laser field drives the system. Our approach is based on the analytical solution of the time-dependent Schrödinger equation by means of considering the bound and scattering states as a composition of two states depending on the relative position of the atoms inside of the molecule, within the framework of both the SFA and SAE approximations. Further, a systematic and analytical way for computing both the bound-free dipole with respect to each center and the rescattering transition matrix elements is developed. This is the advantage of our theoretical model with respect to those used before since it gives a solution free of any artificial and nonphysical effects. In fact, a correct asymptotic behavior for  $\mathbf{R} \rightarrow \infty$  and yet to  $\mathbf{R} \rightarrow 0$  is obtained. In addition, the rescattering transition amplitude is written as a sum of components, obtained from equations which describe each rescattering process (local, nonlocal, and cross) independently.

Our model is an extension and generalization of previous works for atomic systems. It shows that each component contributes, in a different way, to a different region of the ATI spectrum. The results indicate, as expected, that the main contribution to the rescattering transition amplitude corresponds to local events, with the cross and nonlocal terms playing almost no role, when the internuclear distance becomes much larger than the equilibrium one. We should stress, however, that our model is by no means a simple correction to the well-established SFA. Here, we do predict physical processes which were not previously considered, i.e., those modeled by the nonlocal and cross terms, and we do provide methods to identify their contributions, which, at the end can be quite significant for small internuclear distances compared to the equilibrium one. On top of that, our version of

SFA compares very well with the TDSE and the experimental data, which provides an even stringent argument in favor of our model.

In this paper, we used our model for a proof-of-principle that photoelectron spectra contain structural information about the target system. We employ it to retrieve, satisfactorily, the internuclear distance of a  $H_2^+$  molecule using a simple interference equation. The magnitude of the ionization probability for different values of  $R$  was calculated and compared with the TDSE outcomes, and the results present a very good agreement. Both models exhibit the similar behavior: the ionization probability shows the same tendencies, namely, it starts to increase linearly with  $R$  reaching a saturation value from which it remains constant. The comparison of TDSE with SFA, as well as the good agreement between the experiment and the simulations, validates our theoretical model and allows us to believe that extensions to more complicated systems, such as polyatomic molecules with more than three centers, are perfectly feasible. We hope that our work paves the way toward fascinating studies of structural information and charge migrations in the fragmentation processes in large molecules and other complex targets.

**ACKNOWLEDGMENTS**

This work was supported by the project ELI-Extreme Light Infrastructure-phase 2 (Project No. CZ.02.1.01/0.0/0.0/15\_008/0000162) from European Regional Development Fund, Ministerio de Economía y Competitividad through Plan Nacional [Grant No. FIS2011-30465-C02-01, FrOntiers of QUantum Sciences (FOQUS): Atoms, Molecules, Photons and Quantum Information Grants No. FIS2013-46768-P and No. FIS2014-56774-R; and Severo Ochoa Excellence Grant No. SEV-2015-0522], the Catalan Agencia de Gestio d’Ajuts Universitaris i de Recerca (AGAUR) with SGR 874 2014-2016, Fundació Privada Cellex Barcelona and funding from the European Unions Horizon 2020 research and innovation programme under the Marie Skłodowska-Curie Grant Agreement No. 641272 and Laserlab-Europe (Grant No. EU-H2020 654148). N.S. was supported by the Erasmus Mundus Doctorate Program Europhotonics (Grant No. 159224-1-2009-1-FR-ERA MUNDUS-EMJD). N.S., A.C., and M.L. acknowledge ERC AdG OSYRIS and EU FETPRO QUIC. B.W. was supported by AGAUR with a PhD fellowship (Grant No. FI-DGR 2013-2015). J.B. acknowledges Grant No. FIS2014-51478-ERC.

**APPENDIX: TREATMENT OF THE ASYMPTOTIC BEHAVIOR WHEN  $R \rightarrow 0$**

In this appendix we prove, analytically, that our model is capable to satisfy the asymptotic limit when the separation between the two atoms of the molecule is close to zero. For this condition, our model describes a single atom that satisfies the equations previously presented in Ref. [50]. In this sense our theoretical formulation for a diatomic molecule remains compatible with the atomic model.

**1. Bound states and bound-continuum transition matrix element**

When the internuclear distance is close to zero, the bound state of our diatomic molecule is equal to the bound state of an atom,  $\lim_{R \rightarrow 0} \Psi_{0M}(\mathbf{p}) = \Psi_0(\mathbf{p})$ . The wave function describing the bound state for the atomic system [50] reads as

$$\Psi_0(\mathbf{p}) = \frac{\mathcal{N}}{\sqrt{(p^2 + \Gamma^2)(\frac{p^2}{2} + I_p)}}, \tag{A1}$$

where  $\mathcal{N} = [\frac{\sqrt{2I_p}(\Gamma + \sqrt{2I_p})^2}{4\pi^2}]^{1/2}$  is the normalization constant. In order to perform the limit  $R \rightarrow 0$  for the molecular bound state, we are going to use Eq. (37). If we write it as an explicit function of  $\mathbf{R}$  and taking the limit we have

$$\lim_{R \rightarrow 0} \Psi_{0M}(\mathbf{p}) = \lim_{R \rightarrow 0} \left\{ \frac{\mathcal{M} e^{i\frac{R}{2} \cdot \mathbf{p}}}{\sqrt{(p^2 + \Gamma^2)(\frac{p^2}{2} + I_p)}} + \frac{\mathcal{M} e^{-i\frac{R}{2} \cdot \mathbf{p}}}{\sqrt{(p^2 + \Gamma^2)(\frac{p^2}{2} + I_p)}} \right\} = \frac{\lim_{R \rightarrow 0} 2\mathcal{M}}{\sqrt{(p^2 + \Gamma^2)(\frac{p^2}{2} + I_p)}}. \tag{A2}$$

On the other hand, the normalization constant for the molecular bound state is given by Eq. (36) and its limit is

$$\begin{aligned} \lim_{R \rightarrow 0} 2\mathcal{M} &= \lim_{R \rightarrow 0} \frac{1}{\left( \frac{2\pi^2}{(2I_p - \Gamma^2)^2} \left\{ \frac{2e^{-R\Gamma}}{R} - \frac{2e^{-R\sqrt{2I_p}}}{R} \left[ \frac{2\sqrt{2I_p} + R(2I_p - \Gamma^2)}{2\sqrt{2I_p}} \right] + \frac{(\sqrt{2I_p} - \Gamma)^2}{\sqrt{2I_p}} \right\} \right)^{1/2}} \\ &= \lim_{R \rightarrow 0} \frac{1}{\left\{ \frac{2\pi^2}{(2I_p - \Gamma^2)^2} \left[ 2(-\Gamma + \sqrt{2I_p}) - \frac{2I_p - \Gamma^2}{\sqrt{2I_p}} + \frac{(\sqrt{2I_p} - \Gamma)^2}{\sqrt{2I_p}} \right] \right\}^{1/2}} \\ &= \left[ \frac{\sqrt{2I_p}(\sqrt{2I_p} + \Gamma)^2}{4\pi^2} \right]^{1/2} = \mathcal{N}, \end{aligned} \tag{A3}$$

from where the relation  $\lim_{R \rightarrow 0} 2\mathcal{M} = \mathcal{N}$  is demonstrated.

For the bound-continuum transition matrix element, we follow the same analysis. By taking the asymptotic limit as

$$\lim_{\mathbf{R} \rightarrow 0} \mathbf{d}_m(\mathbf{p}_0) = \lim_{\mathbf{R} \rightarrow 0} \{-2i \mathcal{M} \mathcal{A}(\mathbf{p}_0)[e^{\frac{i\mathbf{R}}{2} \cdot \mathbf{p}_0} + e^{-\frac{i\mathbf{R}}{2} \cdot \mathbf{p}_0}]\} = i \mathbf{p}_0 \frac{(p_0^2 + \Gamma^2) + (\frac{p_0^2}{2} + I_p)}{(p_0^2 + \Gamma^2)^{\frac{3}{2}} (\frac{p_0^2}{2} + I_p)^2} \lim_{\mathbf{R} \rightarrow 0} 2\mathcal{M}, \quad (\text{A4})$$

and using Eq. (A3), we obtain

$$\lim_{\mathbf{R} \rightarrow 0} \mathbf{d}_m(\mathbf{p}_0) = i \mathbf{p}_0 \frac{(p_0^2 + \Gamma^2) + (\frac{p_0^2}{2} + I_p)}{(p_0^2 + \Gamma^2)^{\frac{3}{2}} (\frac{p_0^2}{2} + I_p)^2} \mathcal{N}, \quad (\text{A5})$$

which is exactly the bound-continuum transition matrix element for the atomic system, i.e.,

$$\mathbf{d}(\mathbf{p}_0) = i \mathcal{N} \mathbf{p}_0 \frac{(p_0^2 + \Gamma^2) + (\frac{p_0^2}{2} + I_p)}{(p_0^2 + \Gamma^2)^{\frac{3}{2}} (\frac{p_0^2}{2} + I_p)^2}. \quad (\text{A6})$$

## 2. Scattering states and continuum-continuum transition matrix element

For the scattering states, we will prove that  $\lim_{\mathbf{R} \rightarrow 0} \Psi_{\mathbf{M}\mathbf{p}_0}(\mathbf{p}) = \Psi_{\mathbf{p}_0}(\mathbf{p})$ . For the atomic system, the scattering state obeys the equation

$$\Psi_{\mathbf{p}_0}(\mathbf{p}) = \delta(\mathbf{p} - \mathbf{p}_0) + \frac{\mathcal{B}(\mathbf{p}_0)}{\sqrt{p^2 + \Gamma^2(p_0^2 - p^2 + i\epsilon)}}, \quad (\text{A7})$$

where  $\mathcal{B}(\mathbf{p}_0) = -\frac{2\gamma}{(p_0^2 + \Gamma^2)^{\frac{1}{2}}} (1 - \frac{4\pi^2 i\gamma}{|p_0| + i\Gamma})^{-1}$  is the normalization constant.

From Eqs. (41) and (46), the asymptotic limit for the molecular system reads as

$$\begin{aligned} \lim_{\mathbf{R} \rightarrow 0} \Psi_{\mathbf{M}\mathbf{p}_0}(\mathbf{p}) &= \delta(\mathbf{p} - \mathbf{p}_0) + \lim_{\mathbf{R} \rightarrow 0} \left\{ \frac{\mathcal{D}_1(\mathbf{p}_0)[e^{-\frac{i\mathbf{R}}{2} \cdot (\mathbf{p} - \mathbf{p}_0)} + e^{\frac{i\mathbf{R}}{2} \cdot (\mathbf{p} - \mathbf{p}_0)}]}{\sqrt{p^2 + \Gamma^2(p_0^2 - p^2 + i\epsilon)}} - \frac{\mathcal{D}_2(\mathbf{p}_0)[e^{-\frac{i\mathbf{R}}{2} \cdot (\mathbf{p} + \mathbf{p}_0)} + e^{\frac{i\mathbf{R}}{2} \cdot (\mathbf{p} + \mathbf{p}_0)}]}{\sqrt{p^2 + \Gamma^2(p_0^2 - p^2 + i\epsilon)}} \right\} \\ &= \delta(\mathbf{p} - \mathbf{p}_0) + \frac{2 \lim_{\mathbf{R} \rightarrow 0} \{\mathcal{D}_1(\mathbf{p}_0) - \mathcal{D}_2(\mathbf{p}_0)\}}{\sqrt{p^2 + \Gamma^2(p_0^2 - p^2 + i\epsilon)}}. \end{aligned} \quad (\text{A8})$$

Working with the above equation we are going to prove that

$$\mathcal{B}(\mathbf{p}_0) = 2 \lim_{\mathbf{R} \rightarrow 0} \{\mathcal{D}_1(\mathbf{p}_0) - \mathcal{D}_2(\mathbf{p}_0)\}. \quad (\text{A9})$$

Substituting the values of the constants, we have

$$\mathcal{B}(\mathbf{p}_0) = \frac{2\gamma}{\sqrt{p_0^2 + \Gamma^2}} \lim_{\mathbf{R} \rightarrow 0} \left\{ \frac{1 + I_1}{I_2^2 - [1 + I_1]^2} - \frac{I_2}{I_2^2 - [1 + I_1]^2} \right\}. \quad (\text{A10})$$

By taking the limit  $\mathbf{R} \rightarrow 0$  of  $I_2$  and using Eq. (49),

$$\lim_{\mathbf{R} \rightarrow 0} = \frac{-2\pi^2 \gamma}{R(p_0^2 + \Gamma^2 + i\epsilon)} [e^{iR\sqrt{p_0^2 + i\epsilon}} - e^{-R\Gamma}] = \frac{-2\pi^2 \gamma}{\Gamma - i\sqrt{|p_0^2 + i\epsilon|}}, \quad (\text{A11})$$

we find that  $\lim_{\mathbf{R} \rightarrow 0} I_2 = I_1$ . From this last result we can write

$$\mathcal{B}(\mathbf{p}_0) = \frac{2\gamma}{\sqrt{p_0^2 + \Gamma^2}} \left[ \frac{1}{I_1^2 - [1 + I_1]^2} \right] = \frac{-2\gamma}{\sqrt{p_0^2 + \Gamma^2}} [1 + 2I_1]^{-1} = \frac{-2\gamma}{\sqrt{p_0^2 + \Gamma^2}} \left( 1 - \frac{4\pi^2 i\gamma}{|p_0| + i\Gamma} \right)^{-1}, \quad (\text{A12})$$

which is identical to Eq. (33) of Ref. [50].

Concluding the analysis of the diatomic molecular system when  $\mathbf{R} \rightarrow 0$  we proceed to demonstrate that the continuum-continuum molecular matrix element is equal to the continuum-continuum atomic matrix element. The dipole matrix element for the atomic system can be written as

$$\mathbf{g}(\mathbf{p}_1, \mathbf{p}_2) = i\mathcal{B}(\mathbf{p}_2)\mathbf{p}_1 \left\{ \frac{3p_1^2 - p_2^2 + 2\Gamma^2}{(p_1^2 + \Gamma^2)^{\frac{3}{2}} (p_1^2 - p_2^2 + i\epsilon)^2} \right\} - i\mathcal{B}^*(\mathbf{p}_1)\mathbf{p}_2 \left\{ \frac{3p_2^2 - p_1^2 + 2\Gamma^2}{(p_2^2 + \Gamma^2)^{\frac{3}{2}} (p_1^2 - p_2^2 + i\epsilon)^2} \right\}. \quad (\text{A13})$$

Taking the limit in Eq. (53),

$$\begin{aligned} \lim_{\mathbf{R} \rightarrow 0} \mathbf{g}_m(\mathbf{p}_1, \mathbf{p}_2) &= 2 \lim_{\mathbf{R} \rightarrow 0} [\mathcal{Q}_1(\mathbf{p}_1, \mathbf{p}_2) + \mathcal{Q}_2(\mathbf{p}_1, \mathbf{p}_2)] \\ &= iC_1(\mathbf{p}_1, \mathbf{p}_2) 2 \lim_{\mathbf{R} \rightarrow 0} \left[ \frac{1 + I_1}{I_2^2 - [1 + I_1]^2} - \frac{I_2}{I_2^2 - [1 + I_1]^2} \right]_{p_2} \\ &\quad - iC_2(\mathbf{p}_1, \mathbf{p}_2) 2 \lim_{\mathbf{R} \rightarrow 0} \left[ \frac{1 + I_1}{I_2^2 - [1 + I_1]^2} - \frac{I_2}{I_2^2 - [1 + I_1]^2} \right]_{p_1}^*, \end{aligned} \quad (\text{A14})$$

where

$$\lim_{\mathbf{R} \rightarrow 0} \mathbf{g}_m(\mathbf{p}_1, \mathbf{p}_2) = iC_1(\mathbf{p}_1, \mathbf{p}_2) \left\{ \frac{2\gamma}{\sqrt{p_2^2 + \Gamma^2}} \lim_{\mathbf{R} \rightarrow 0} \left[ \frac{1}{I_1^2 - [1 + I_1]^2} \right]_{p_2} \right\} - iC_2(\mathbf{p}_1, \mathbf{p}_2) \left\{ \frac{2\gamma}{\sqrt{p_1^2 + \Gamma^2}} \lim_{\mathbf{R} \rightarrow 0} \left[ \frac{1}{I_1^2 - [1 + I_1]^2} \right]_{p_1}^* \right\}. \quad (\text{A15})$$

By following the same procedure as in Eq. (A12), we finally obtain that

$$\mathcal{B}(\mathbf{p}_2) = \left\{ \frac{2\gamma}{\sqrt{p_2^2 + \Gamma^2}} \lim_{\mathbf{R} \rightarrow 0} \left[ \frac{1}{I_1^2 - [1 + I_1]^2} \right]_{p_2} \right\} \quad (\text{A16})$$

and

$$\mathcal{B}^*(\mathbf{p}_1) = \left\{ \frac{2\gamma}{\sqrt{p_1^2 + \Gamma^2}} \lim_{\mathbf{R} \rightarrow 0} \left[ \frac{1}{I_1^2 - [1 + I_1]^2} \right]_{p_1}^* \right\}. \quad (\text{A17})$$

Grouping conveniently the above equations we get

$$\lim_{\mathbf{R} \rightarrow 0} \mathbf{g}_m(\mathbf{p}_1, \mathbf{p}_2) = i\mathcal{B}(\mathbf{p}_2)\mathbf{p}_1 \left\{ \frac{3p_1^2 - p_2^2 + 2\Gamma^2 - i\epsilon}{(p_1^2 + \Gamma^2)^{\frac{3}{2}}(p_1^2 - p_2^2 + i\epsilon)^2} \right\} - i\mathcal{B}^*(\mathbf{p}_1)\mathbf{p}_2 \left\{ \frac{3p_2^2 - p_1^2 + 2\Gamma^2 + i\epsilon}{(p_2^2 + \Gamma^2)^{\frac{3}{2}}(p_1^2 - p_2^2 + i\epsilon)^2} \right\}, \quad (\text{A18})$$

which is nothing else than the atomic transition matrix continuum-continuum element [see Eq. (37) of Ref. [50]].

We have indeed demonstrated, with the above analysis and relations, that the theoretical model presented in this contribution configures a general model which not only describes the ATI process in diatomic molecules, but is also able, when the appropriate limits are taken, to model the atomic ATI.

- 
- [1] P. B. Corkum, Plasma Perspective on Strong-Field Multiphoton Ionization, *Phys. Rev. Lett.* **71**, 1994 (1993).
- [2] S. Baker, J. S. Robinson, C. A. Haworth, H. Teng, R. A. Smith, C. C. Chirilă, M. Lein, J. W. G. Tisch, and J. P. Marangos, Probing proton dynamics in molecules on an attosecond time scale, *Science* **312**, 424 (2006).
- [3] Y. Mairesse, D. Zeidler, N. Dudovich, M. Spanner, J. Levesque, D. M. Villeneuve, and P. B. Corkum, High-Order Harmonic Transient Grating Spectroscopy in a Molecular Jet, *Phys. Rev. Lett.* **100**, 143903 (2008).
- [4] H. J. Wörner, J. B. Bertrand, D. V. Kartashov, P. B. Corkum, and D. M. Villeneuve, Following a chemical reaction using high-harmonic interferometry, *Nature (London)* **466**, 604 (2010).
- [5] T. Zuo, A. D. Bandrauk, and P. B. Corkum, Laser-induced electron diffraction: A new tool for probing ultrafast molecular dynamics, *Chem. Phys. Lett.* **259**, 313 (1996).
- [6] M. Lein, Molecular imaging using recolliding electrons, *J. Phys. B: At., Mol. Opt. Phys.* **40**, R135 (2007).
- [7] M. Meckel, A. Staudte, S. Patchkovskii, D. M. Villeneuve, P. B. Corkum, R. Dörner, and M. Spanner, Signatures of the continuum electron phase in molecular strong-field photoelectron holography, *Nat. Phys.* **10**, 594 (2014).
- [8] J. Itatani, J. Levesque, D. Zeidler, H. Niikura, H. Pépin, J. C. Kieffer, P. B. Corkum, and D. M. Villeneuve, Tomographic imaging of molecular orbitals, *Nature (London)* **432**, 867 (2004).
- [9] S. Patchkovskii, Z. Zhao, T. Brabec, and D. M. Villeneuve, High Harmonic Generation and Molecular Orbital Tomography in Multielectron Systems: Beyond the Single Active Electron Approximation, *Phys. Rev. Lett.* **97**, 123003 (2006).
- [10] M. Lewenstein, Ph. Balcou, M. Y. Ivanov, A. L'Huillier, and P. B. Corkum, Theory of high-harmonic generation by low-frequency laser fields, *Phys. Rev. A* **49**, 2117 (1994).
- [11] J. L. Krause, K. J. Schafer, and K. C. Kulander, High-Order Harmonic Generation from Atoms and Ions in the High Intensity Regime, *Phys. Rev. Lett.* **68**, 3535 (1992).
- [12] K. C. Kulander, K. J. Schafer, and K. L. Krause, in *Super-Intense Laser Atom Physics* edited by B. Piraux, A. L'Huillier, and K. Rzażewski, NATO Advanced Studies Institute Series B: Physics, Vol. 316 (Plenum, New York, 1993), p. 95
- [13] O. Smirnova and M. Ivanov, in *Attosecond and XUV Physics: Ultrafast Dynamics and Spectroscopy*, edited by T. Schultz and M. Vrakking (Wiley, Weinheim, Germany, 2014).
- [14] O. Smirnova, Y. Mairesse, S. Patchkovskii, N. Dudovich, D. Villeneuve, P. Corkum, and M. Y. Ivanov, High harmonic interferometry of multi-electron dynamics in molecules, *Nature (London)* **460**, 972 (2009).
- [15] S. Haessler, J. Caillat, W. Boutu, C. Giovanetti-Teixeira, T. Ruchon, T. Auguste, Z. Diveki, P. Breger, A. Maquet, B. Carré

- et al.*, Attosecond imaging of molecular electronic wavepackets, *Nat. Phys.* **6**, 200 (2010).
- [16] B. K. McFarland, J. P. Farrell, P. H. Bucksbaum, and M. Gühr, High harmonic generation from multiple orbitals in  $N_2$ , *Science* **322**, 1232 (2008).
- [17] Z. Diveki, R. Guichard, A. Camper, S. Haessler, T. Auguste, T. Ruchon, B. Carré, A. Maquet, and R. Taïeb, Molecular orbital tomography from multi-channel harmonic emission in  $N_2$ , *Chem. Phys.* **414**, 121 (2012).
- [18] C. Wang, M. Okunishi, X. Hao, Y. Ito, J. Chen, Y. Yang, R. R. Lucchese, M. Zhang, B. Yan, W. D. Li, D. Ding, and K. Ueda, Resonancelike enhancement in high-order above-threshold ionization of polyatomic molecules, *Phys. Rev. A* **93**, 043422 (2016).
- [19] Y. Zhou, O. I. Tolstikhin, and T. Morishita, Near-Forward Rescattering Photoelectron Holography in Strong-Field Ionization: Extraction of the Phase of the Scattering Amplitude, *Phys. Rev. Lett.* **116**, 173001 (2016).
- [20] M. Meckel, D. Comtois, D. Zeidler, A. Staudte, D. Pavičić, H. C. Bandulet, H. Pépin, J. C. Kieffer, R. Dörner, D. M. Villeneuve, and P. B. Corkum, Laser-induced electron tunneling and diffraction, *Science* **320**, 1478 (2008).
- [21] D. B. Milošević, G. G. Paulus, D. Bauer, and W. Becker, Above-threshold ionization by few-cycle pulses, *J. Phys. B: At., Mol. Opt. Phys.* **39**, R203 (2006).
- [22] G. N. Gibson and J. Biegert, Influence of orbital symmetry on high-order-harmonic generation and quantum tomography, *Phys. Rev. A* **78**, 033423 (2008).
- [23] S. Odžak and D. B. Milošević, Interference effects in high-order harmonic generation by homonuclear diatomic molecules, *Phys. Rev. A* **79**, 023414 (2009).
- [24] A. Li, J. Wang, N. Ren, P. Wang, W. Zhu, X. Li, R. Hoehn, and S. Kais, The interference effect of laser-assisted bremsstrahlung emission in coulomb fields of two nuclei, *J. Appl. Phys.* **114**, 124904 (2013).
- [25] M. Qin, X. Zhu, K. Liu, Q. Zhang, and P. Lu, Imprints of the molecular-orbital geometry on the high-harmonic ellipticity, *Opt. Express* **18**, 20181 (2012).
- [26] S. Odžak and D. B. Milošević, Dressed-bound-state molecular strong-field approximation: Application to high-order harmonic generation by heteronuclear diatomic molecules, *J. Opt. Soc. Am. B* **29**, 2147 (2012).
- [27] N. Nguyen and V. Le, Retrieval of interatomic separations of complex molecules by ultra-short laser pulses, *Comput. Theor. Chem.* **964**, 12 (2011).
- [28] E. Hijano, C. Serrat, G. N. Gibson, C. Figueira de Morisson Faria, and J. Biegert, Retrieval of interatomic separations of complex molecules by ultra-short laser pulses, *J. Mod. Opt.* **58**, 1166 (2011).
- [29] C. Figueira de Morisson Faria and B. B. Augstein, Molecular high-order harmonic generation with more than one active orbital: Quantum interference effects, *Phys. Rev. A* **81**, 043409 (2010).
- [30] E. Hijano, C. Serrat, G. N. Gibson, and J. Biegert, Orbital geometry determined by orthogonal high-order harmonic polarization components, *Phys. Rev. A* **81**, 041401 (2010).
- [31] M. Lein, J. P. Marangos, and P. L. Knight, Electron diffraction in above-threshold ionization of molecules, *Phys. Rev. A* **66**, 051404 (2002).
- [32] C. D. Lin, A. T. Le, Z. Chen, T. Morishita, and R. R. Lucchese, Strong-field re-scattering physics-self-imaging of a molecule by its own electrons, *J. Phys. B: At., Mol. Opt. Phys.* **43**, 122001 (2010).
- [33] C. I. Blaga, J. Xu, A. D. DiChiara, E. Sistrunk, K. Zhang, P. Agostini, T. A. Miller, L. F. DiMauro, and C. D. Lin, Imaging ultrafast molecular dynamics with laser-induced electron diffraction, *Nature (London)* **483**, 194 (2012).
- [34] M. G. Pullen, B. Wolter, A. T. Le, M. Baudisch, M. Hemmer, A. Senftleben, C. D. Schröter, J. Ullrich, R. Moshhammer, C. D. Lin, and J. Biegert, Imaging an aligned polyatomic molecule with laser-induced electron diffraction, *Nat. Commun.* **6**, 7262 (2015).
- [35] Y. Ito, C. Wang, A-T. Le, M. Okunishi, D. Ding, C. D. Lin, and K. Ueda, Extracting conformational structure information of benzene molecules via laser-induced electron diffraction, *Struct. Dyn.* **3**, 034303 (2016).
- [36] P. Salières, B. Carré, L. L. Déroff, F. Grasbon, G. G. Paulus, H. Walther, R. Kopold, W. Becker, D. B. Milošević, A. Sanpera, and M. Lewenstein, Feynman's path-integral approach for intense-laser-atom interactions, *Science* **292**, 902 (2001).
- [37] J. Xu, C. I. Blaga, K. Zhang, Y. H. Lai, C. D. Lin, T. A. Miller, P. Agostini, and L. F. DiMauro, Diffraction using laser-driven broadband electron wave packets, *Nat. Commun.* **5**, 4635 (2014).
- [38] D. B. Milošević, Strong-field approximation for ionization of a diatomic molecule by a strong laser field, *Phys. Rev. A* **74**, 063404 (2006).
- [39] E. V. van der Zwan and M. Lein, Molecular Imaging using High-Order Harmonic Generation and above-Threshold Ionization, *Phys. Rev. Lett.* **108**, 043004 (2012).
- [40] H. Hetzheim, C. Figueira de Morisson Faria, and W. Becker, Interference effects in above-threshold ionization from diatomic molecules: Determining the internuclear separation, *Phys. Rev. A* **76**, 023418 (2007).
- [41] M. F. Ciappina, C. C. Chirilă, and M. Lein, Influence of Coulomb continuum wave functions in the description of high-order harmonic generation with  $H_2^+$ , *Phys. Rev. A* **75**, 043405 (2007).
- [42] C. C. Chirilă and M. Lein, Strong-field approximation for harmonic generation in diatomic molecules, *Phys. Rev. A* **73**, 023410 (2006).
- [43] M. Busladžić, A. Gazibegović-Busladžić, D. B. Milošević, and W. Becker, Angle-Resolved High-Order above-Threshold Ionization of a Molecule: Sensitive Tool for Molecular Characterization, *Phys. Rev. Lett.* **100**, 203003 (2008).
- [44] M. F. Ciappina and W. R. Cravero, Two center and coulomb effects in near-threshold ionization of  $H_2^+$  by short laser pulses, *J. Mod. Opt.* **56**, 11 (2009).
- [45] J. Bauer, Coulomb-corrected strong-field approximation for the two-electron atom, *Phys. Rev. A* **55**, 3261 (1997).
- [46] S. V. Popruzhenko, G. G. Paulus, and D. Bauer, Coulomb-corrected quantum trajectories in strong-field ionization, *Phys. Rev. A* **77**, 053409 (2008).
- [47] C. J. Joachain, N. J. Kylstra, and R. M. Potvliege, *Atoms in Intense Laser Fields* (Cambridge University Press, Cambridge, UK, 2011).
- [48] W. Becker, S. Long, and J. K. McIver, Higher-harmonic production in a model atom with short-range potential, *Phys. Rev. A* **41**, 4112 (1990).

- [49] M. Lewenstein, K. C. Kulander, K. J. Schafer, and P. H. Bucksbaum, Rings in above-threshold ionization: A quasiclassical analysis, *Phys. Rev. A* **51**, 1495 (1995).
- [50] N. Suárez, A. Chacón, M. F. Ciappina, J. Biegert, and M. Lewenstein, Above-threshold ionization and photoelectron spectra in atomic systems driven by strong laser fields, *Phys. Rev. A* **92**, 063421 (2015).
- [51] L. V. Keldysh, Ionization in the field of a strong electromagnetic wave, *Zh. Eksp. Teor. Fiz.* **47**, 1945 (1965) [*Sov. Phys.–JETP* **20**, 1307 (1965)].
- [52] F. H. M. Faisal, Multiple absorption of laser photons by atoms, *J. Phys. B: At. Mol. Phys.* **6**, L89 (1973).
- [53] H. R. Reiss, Effect of an intense electromagnetic field on a weakly bound system, *Phys. Rev. A* **22**, 1786 (1980).
- [54] J. Grochmalicki, J. R. Kukliński, and M. Lewenstein, Above-threshold ionisation and electron scattering in intense laser fields, *J. Phys. B: At. Mol. Phys.* **19**, 3649 (1986).
- [55] L. Elsgoltz, *Differential Equations and the Calculus of Variations* (University Press of the Pacific, Miami, 2003).
- [56] F. Ehlotzky, Harmonic generation in keldysh-type models, *Nuovo Cimento*. **14**, 517 (1992).
- [57] H. Goldstein, C. Poole, and J. Safko, *Classical Mechanics*, 3rd ed. (Addison Wesley, San Francisco, 2002), p. 356.
- [58] Nist standard reference data program, <http://webbook.nist.gov/cgi/cbook.cgi?ID=C12184906&Units=SI>.
- [59] B. Chapman, G. Jost, and R. Van Der Pas, *Using OpenMP: Portable Shared Memory Parallel Programming* (MIT Press, Cambridge, MA, 2007).
- [60] E. Gabriel, G. E. Fagg, G. Bosilca, T. Angskun, J. J. Dongarra, J. M. Squyres, V. Sahay, P. Kambadur, B. Barrett, A. Lumsdaine, R. H. Castain, D. J. Daniel, R. L. Graham, and T. S. Woodall, Open MPI: Goals, concept, and design of a next generation MPI implementation, in *Proceedings, 11th European PVM/MPI Users' Group Meeting, Budapest, Hungary* (Springer, Berlin, 2004), pp. 97–104.
- [61] M.G. Pullen, B. Wolter, A.T. Le, M. Baudisch, M. Sclafani, H. Pires, C.D. Schröter, J. Ullrich, R. Moshhammer, T. Pfeifer, C. D. Lin, and J Biegert, Influence of orbital symmetry on diffraction imaging with rescattering electron wave packets, *Nat. Commun.* **7**, 11922 (2016).
- [62] M. Magrakvelidze, C. M. Aikens, and U. Thumm, Dissociation dynamics of diatomic molecules in intense laser fields: A scheme for the selection of relevant adiabatic potential curves, *Phys. Rev. A* **86**, 023402 (2012).